AN ACTIVE ROCKET LAUNCHER DESIGN FOR AN ATTACK HELICOPTER

A THESIS SUBMITTED TO
THE GRADUATE SCHOOL OF NATURAL AND APPLIED SCIENCES
OF
MIDDLE EAST TECHNICAL UNIVERSITY

BY

TUNÇ BARAN MERİÇ

IN PARTIAL FULFILLMENT OF THE REQUIREMENTS
FOR
THE DEGREE OF MASTER OF SCIENCE
IN
AEROSPACE ENGINEERING

FEBRUARY 2018

Approval of the thesis:

AN ACTIVE ROCKET LAUNCHER DESIGN FOR AN ATTACK HELICOPTER

submitted by **TUNÇ BARAN MERİÇ** in partial fulfillment of the requirements for the degree of **Master of Science in Aerospace Engineering Department, Middle East Technical University** by,

Prof. Dr. Gülbin Dural Ünver
Dean, Graduate School of **Natural and Applied Sciences**

Prof. Dr. Ozan Tekinalp
Head of Department, **Aerospace Engineering**

Asst. Prof. Dr. Ali Türker Kutay
Supervisor, **Aerospace Engineering Department, METU**

Examining Committee Members:

Prof. Dr. Ozan Tekinalp _______________
Aerospace Engineering Department, METU

Assoc. Prof. Dr. ˙Ilkay Yavrucuk _______________
Aerospace Engineering Department, METU

Assoc. Prof. Dr. Coşku Kasnakoğlu _______________
Electrical and Electronics Engineering Department, TOBB ETU

Asst. Prof. Dr. Ali Türker Kutay _______________
Aerospace Engineering Department, METU

Asst. Prof. Dr. Durdu Hakan Utku _______________
Industrial Engineering Department, UTAA

Date: _______________

I hereby declare that all information in this document has been obtained and presented in accordance with academic rules and ethical conduct. I also declare that, as required by these rules and conduct, I have fully cited and referenced all material and results that are not original to this work.

Name, Last Name : Tunç Baran MERİÇ

Signature :

DISCLAIMER

THE OPINIONS AND CONCLUSIONS EXPRESSED HEREIN ARE THOSE OF THE INDIVIDUAL STUDENT AUTHOR AND DO NOT NECESSARILY REPRESENT THE VIEWS OF EITHER THE TURKISH LAND FORCES OR ANY OTHER GOVERNMENTAL AGENCY.

ABSTRACT

AN ACTIVE ROCKET LAUNCHER DESIGN FOR AN ATTACK HELICOPTER

Meriç, Tunç Baran
M.S., Department of Aerospace Engineering
Supervisor: Asst. Prof. Dr. Ali Türker KUTAY

February 2018, 71 Pages

In this thesis, an active rocket launcher is designed to automate the firing unguided rockets on helicopter. The proposed approach includes determination of the rocket launch angle through a regression model, eliminating the need for the pilot to study pitch delivery charts. Also, an active launcher is proposed that can be tilted with respect to helicopter body. The launcher allows the desired launch angle to be satisfied without changing the helicopter pitch attitude. The proposed launcher reduces pilot workload and preparation time significantly and increases the possibility of launching the rocket at an optimal angle without affecting helicopter flight condition.

Keywords: Helicopter, Rocket Launcer, Regression Analysis, PID Controller, Simulation,

ÖZ

TAARRUZ HELİKOPTERİ İÇİN AKTİF ROKET LANÇERİ TASARIMI

Meriç, Tunç Baran
Yüksek Lisans, Havacılık ve Uzay Mühendisliği Bölümü
Tez Yöneticisi: Yrd.Doç. Dr. Ali Türker KUTAY

Şubat 2018, 71 Sayfa

Bu tezde, helikopter ile roket atışını otomatikleştirecek bir yöntem tasarlanmıştır. Sunulan yaklaşım, roket atış açısının regresyon modeli ile hesaplayarak pilotun roket yükseliş açısı atım kartlarına çalışmasına gerek bırakmayacak yöntemi içermektedir. Ayrıca aktif lançer, helikopterin gövdesine göre açısı değişecek şekilde sunuşlmuştur. Lançer, helikopterin yunuslama ekseninde değişiklik olmadan gerekli açıyı sağlamaktadır. Sunulan lançer, pilotun iş yükünü ve hazırlık zamanını önemli derecede azaltmakta ve helikopterin uçuş durumunu etkilemeden roketin en uygun açıyla atılması olasığını arttırmaktadır.

Anahtar Kelimeler: Helikopter, Roket Lançeri, Regresyon Analizi, PID Kontrolcü, Simülasyon

dedicated to martyred pilots of Attack Helicopter Battalion…

ACKNOWLEDGMENTS

Ali Türker KUTAY, Asst. Prof.Dr. at Department of Aerospace Engineering METU, his leading guidance, encouragement, and continuous support from beginning to the end of my M.S. study.

İlkay YAVRUCUK, Assoc. Prof.Dr. at Department of Aerospace Engineering METU, for giving permission to use the simulator,

Sarper KUMBASAR, Modelling and Simulation Engineer at ROKETSAN Missiles Inc., for his precious advice and feedbacks about this study,

Osman AKGÜN and Yusuf ELMAS, consultants at TUBITAK Space Research Institute, for their excellent work in physical and dynamic modeling of the rocket and the launcher,

Bulut Efe AKMENEK, researcher at Department of Aerospace Engineering METU, for his great support in integrating the system into the simulation,

And all personnel of Attack Helicopter Batallion for their glorious support and motivation.

Finally, many thanks to my family,and my beloved for their endless love, support, encouragement and their trust in me.

TABLE OF CONTENTS

LIST OF TABLES

TABLES

LIST OF FIGURES

FIGURES

CHAPTER 1

INTRODUCTION

The author has worked in Turkish Land Forces (TLF) as an attack helicopter pilot (900 flight hours) for over four years. Regarding his experiences as well as his colleagues' views, this study aims to demonstrate and examine the problems that attack helicopters encounter when they use unguided rockets in a conflict area. Also, a different concept of the unguided rocket launcher is proposed that will automate the pitch angle to satisfy the elevation for high hit probability and high kill ratio. The proposed approach includes determination of the rocket launch angle through a polynomial regression model, eliminating the need for the pilot to consider pitch delivery charts. The launcher will allow the desired launch angle to be satisfied without changing the helicopter pitch attitude.

1.1 Weapons and Tactics

There are several kinds of attack helicopters in Turkish Land Forces (TLF) inventory, two of which are the T-129T ATAK developed by Turkish Aerospace Industry (TAI) and the AH-1W Super Cobra developed by Bell Helicopter. This section intends to familiarize the reader with the abilities and inadequacies of the weapon systems and current usage tactics, especially regarding the AH-1W, as that is the author's primary helicopter.

1.1.1 Unguided 2.75-Inch Rocket

Both helicopters utilize 70-mm (2.75-inch) unguided rockets as one of the primary weapon

systems in air-to-ground missions. In this thesis, a 70-mm rocket system for the AH-1W is examined and demonstrated. The LAU 68A tube launcher shown in Figure 1, which can carry seven rockets, is modeled for this study.

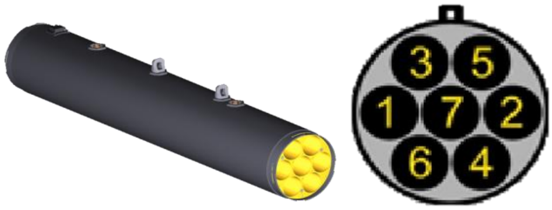

Figure 1: LAU 68A Tube Launcher [Office of the Chief of Naval Operations, 2008]

Hydra-70 rockets, which are 70-mm fin-stabilized unguided rockets, can be launched from this launcher. An MK-66 rocket motor is used as the propellant, and with the motor, the rocket has an 8,000-meter maximum range. The warhead for the Hydra-70 rocket M151 is extensively employed in TLF. A firing instant in a Cobra cockpit is shown in Figure 2.

Figure 2: Rocket Firing

The rocket is a simple and relatively inexpensive weapon in contrast with guided munitions. They are all passive systems and laser illumination or wire guidance is not required. Also, they can be extremely lethal upon impact and allow pilots to quickly respond to hostile fire within the effective range of the munitions onboard the helicopter [1]. Conversely, manufacturing tolerances, aiming inaccuracies and external disturbances significantly limit rocket accuracy [2].

The primary reference of army aviators for combat tactics , “Tactical Employment AH-1W(U) [3],” clearly states how to use unguided weapons for the AH-1W Super Cobra. The weapons delivery profiles are given as “Diving Fire,” “Running Fire,” “Hover Fire,” and “Low Altitude Pop-Up Fire” [3]. The most common rocket firing technique attack pilots use in a combat zone is low altitude pop-up fire. While the target is in at least a 2,000-meter range, the pilot starts the pop-up maneuver and gains 300–600 feet above ground level (AGL), then dives, nose down, and begins shooting as shown in Figure 3. It is also stated that with this technique, the circular error of probability (CEP) will be reduced and accuracy will be increased [3].

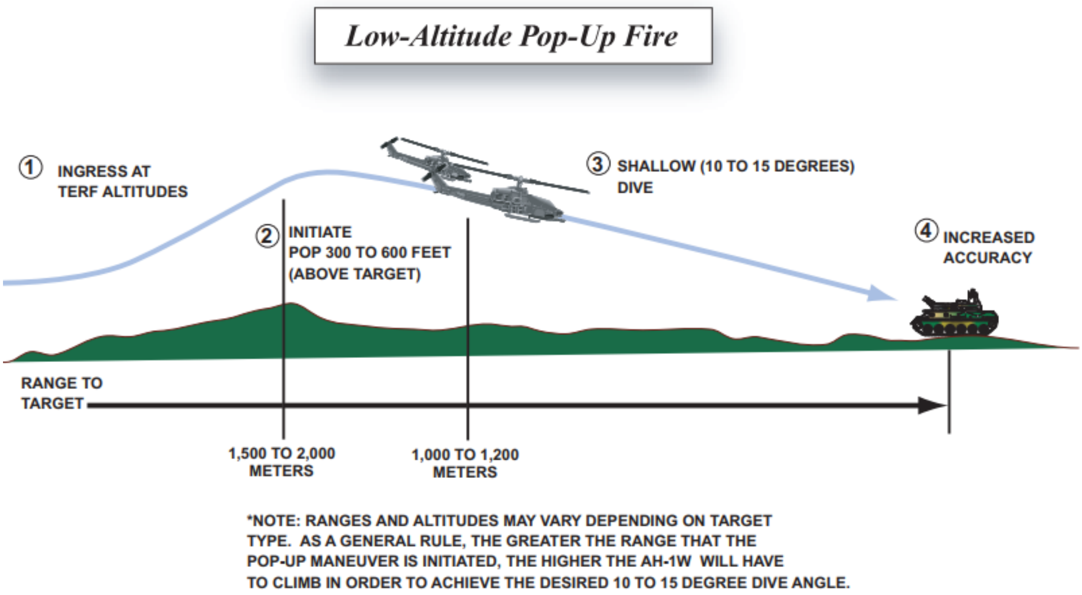

Figure 3: Pop-Up Fire [Office of the Chief of Naval Operations, 2003]

The reticle calibration used by pilots for aiming rockets is stated below:

> *The rocket reticle is calibrated for 100 knots, level delivery, and automatically adjusts for changing airspeed. For this method to be accurate, the pilot must be sure to be on altitude and at the desired*

range. Once at the range dialed in, the pilot centers the target in the rocket reticle and fires. If above or below 100 feet above the target's altitude, the pilot will have to make an appropriate djustment. If below 100 feet, the rocket shots will be short and if above 100 feet, the rocket shots will be long.[3]

As indicated, for proper and accurate rocket firing, the velocity must be 100 knots, and the height between the target and the helicopter must be exactly 100 feet. Any deviations from these values can cause the rocket to miss the target. Also, for an exact range estimation, the gunner or copilot should apply laser range finding; by this method, the reticle updates itself for the new estimated range. The primary variables of the rocket delivery—airspeed, altitude, and range—depend on the two pilots' mutual work, handling qualities, and cockpit coordination. This means more workload for the pilots.

1.1.2 TOW Missile

The tube-launched, optically tracked, wire-guided (TOW) missile is a relatively low-speed, anti-armor missile that is commonly used in combat. The respective work of both pilot and copilot is needed to use the TOW missile system in the helicopter. While the pilot tries to maintain the helicopter's attitude to achieve a stable firing condition, the copilot/gunner manually aims the reticle on the target with a controller called "sight hand control" [4] During the flight time of the missile, the helicopter is exposed and vulnerable to hostile fire. Being revealed to enemy lines for around 20 seconds comprises high risk for the crew, and being shot down is possible during the engagement. To diminish this risk, the wingman tries to cover the helicopter, sometimes with suppressive fire on the target. Also, the firing helicopter pilot can attempt to suppress the enemy with his/her 20-millimeter gun, using a helmet-mounted sight. A TOW target engagement photo is shown in Figure 4.

Figure 4: TOW Firing

1.1.3 Hellfire Missile

The Hellfire missile is a semi-active, 8,000-meter-ranged, laser-guided precision weapon. During the missile flight, the target needs to be illuminated with a laser. For this purpose, there are three alternative methods. The gunner illuminates the target with a similar method to that mentioned in the TOW section, the wingman illuminates the target with his/her laser designator, or a ground unit can illuminate the target with a suitable designator. In all cases, the target must be illuminated and be tracked during at least the last part of the missile's flight on the way to the target. If the missile loses the laser spot on the target, it may miss. In contrast to TOW missiles, an enemy platform with a laser warning system can sense laser illumination on itself and can then fire back.

1.2 Problem Statements

The desired launch angle of the rocket is determined based on several factors: the relative position of the target, the speed of the helicopter, altitude, and temperature.

When firing conventional rockets, pilots have to use pitch delivery charts and graphs provided to aid in preflight preparations and during flight operations. First, the pilot selects the appropriate chart for the type of fire, running or hover, and for the altitude and speed of the helicopter. The pilot then examines the elevation and range of the target to calculate the correct pitch angle. The procedure for finding the right launch angle brings an extra burden on the pilot, which can be critical during operations. Also, during the engagement, even a minor forward cyclic error can cause an undesirable pitch down such that the desired angle cannot be provided and the rocket may miss the target. Because the process depends on well-established rules and does not require human intelligence, it can be safely automated to reduce workload in the cockpit. An example of pitch delivery chart is given in Figure 5.

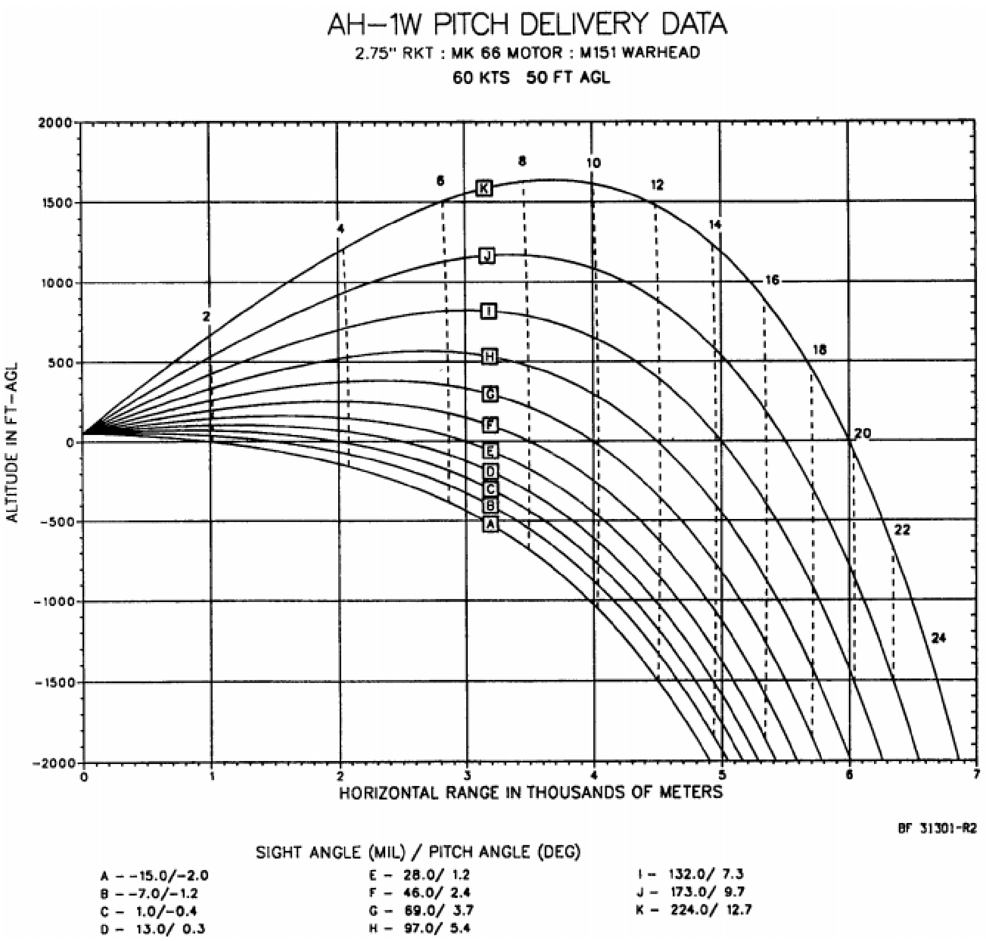

Figure 5: Rocket Delivery Chart [Office of the Chief of Naval Operations, 2008]

Another difficulty in a traditional rocket launch system where the launcher is fixed to the helicopter body is that it is the pilot's responsibility to adjust the helicopter attitude to bring the rocket to the desired angle for launch. Aside from requiring the pilot's attention, changing the helicopter's attitude may change the airspeed, and this situation can be undesirable in hostile territory. Notably, when the flight condition

changes, the previously calculated launch angle for initial flight conditions may not be the optimal angle anymore. Consequently, the pilot needs to either recalculate the launch angle, spending precious time in a combat environment, or fire the rocket with a suboptimal angle, reducing the chances of successful target engagement.
All guided weapons except passive homing missiles cause a helicopter in combat to be exposed for a while. The author endorses the opinion of Haney [5] about the usage of precision-guided missiles.

> *Ideally, every pilot would prefer a missile system that allowed him to "fire and forget" the missile after launch. This allows the pilot to fire the missile similar to shooting a rocket or bullet and to egress from the objective area, rather than continuing to track the missile all the way to target impact.*

1.3 Literature Review

The stability and accuracy of the rockets launched from helicopters have been studied many times. These studies are led by military authorities, helicopter pilots, or the organizations under contract. Some of these studies are presented by other researchers. A study by Morse [6] focuses on the effects of unsteady wake flow, and the velocity gradients of the rotor's free-stream wake boundary in considering automatic fire control systems and their potential for improved, cost-effective delivery of helicopter-launched rocket systems. Additionally, Jenkins [7] studied the effects of rotor downwash and recommends accuracy improvements for the low-speed launch of 2.75-inch rockets.

Osder, Douglas, and Company [8] studied integrated flight and fire control modes used in fixed-wing platforms of attack helicopters for improving combat effectiveness, weapon accuracy, and survivability. Similarly, a study by Blakelock [9] integrates stability and augmentation systems with the movable gun.

In an article entitled “The optimal control and correction of a three-axis gyroscopic platform fixed on the board of a flying object,” Koruba [10] concludes that stabilization of motion and disturbances affect the particular platform. Further, Koruba, Dziopa, and Krzysztofik [11] studied ground platform dynamics and controls of the gyroscope-stabilized platform in a surface-to-air missile system [12], using modern control methods such as LQR. The proposed methods can be utilized in either weapons systems or surveillance systems.

Parkpoom and Narongkorn [13] focused on multiple-launch rocket system angle controls. In this study, they implemented a proportional–integral–derivative (PID) controller for yaw control of the system. Similarly, Özdemir [14] designed a PID controller for gun and/or sight stabilization of a turret subsystem and tuned the gains using a multilayered back-propagation neural network called the neural PID tuner. Lastly, Kapulu [15] modeled and simulated 2.75-inch rocket launchers and examined the effect of rotor downwash on rocket range. Her study also investigated safe jettison ranges of wing stores.

1.4 The Objectives of the Thesis

Pilots always prefer using “fire and forget” missiles because of the high survivability for the designator. The rockets are not an exact alternative for those precision-guided missiles that have high kill ratios and armor penetration abilities, but their simplicity of use and ease of manufacturing, in addition to the lack of any available countermeasures, make these rockets indispensable. To handle inaccuracy problems, Joyce suggests an improved training system for gunnery. However, the author disagrees with Joyce’s statement that “advances in technology must continue to remain dominant, but must not become the sole solution to every problem” [1]. This study is used as a foundation upon which to identify the technology that can assist in the accuracy of unguided rockets. In this thesis, an active rocket launcher was designed to automate the described procedure. The proposed approach includes determination of the rocket launch angle through a regression model, eliminating the need for the pilot to study pitch delivery charts. In addition, an active launcher is proposed that can be tilted with respect to the helicopter body, which would allow achieving the desired launch angle without changing the helicopter pitch attitude. The proposed launcher significantly reduces pilot workload and preparation time and increases the possibility of launching the rocket at an optimal angle without affecting helicopter flight conditions. The performance of the proposed launcher was compared with the existing literature as well as being compared to a conventional fixed launcher by simulating multiple firings of both types of launchers.

1.5 The Scope of the Thesis

In the Introduction, the aim and purpose of the study are described. The second chapter includes the procedure for automation of a required pitch delivery angle for the active rocket launcher. The third chapter explains the methods for the required dynamic model of the M260 rocket launcher. The fourth chapter gives information about the simulation setup, the process of testing, and the results achieved with the active rocket launcher system. Finally, the conclusion and potential future studies are discussed in the fifth chapter.

CHAPTER 2

ROCKET DELIVERY MODEL

In this section, the procedure for automation of a required pitch delivery angle with the active rocket launcher is described. The proposed approach includes determination of the rocket launch angle through a regression model, eliminating the need for the pilot to study pitch delivery charts.

The data set required to build the polynomial regression model was obtained and produced from the simulation runs. The simulation parameter intervals are given in Table 1.

Table 1: Parameter Intervals

Parameter	**Min.**	**Max.**	**Sample Size**
Air Density (kg/m^3)	0.800	1.395	8
Air Velocity (IAS) (knots)	0	120	3
Vertical Distance Between Target and Helicopter (meters)	15.24	609.6	14
Required Pitch Angle (degrees)	−8	18	27
Horizontal Distance Between Target and Helicopter (meters)	211.13	9452.41	9079

A mathematical model, given in Section 2.4, was used to obtain the flight trajectory of the rocket using the various parameters shown in Table 1. With the help of this model, a new data set was obtained by multiplication of each assigned parameters shown in Table 1, resulting in five columns and 27,216 rows. The identities of the data are given in Table 2. For given parameter intervals, hit distances were calculated, and a sample of the results is shown in Table 3.

Table 2: Parameters of the Data

Parameter	**Unit**	**Notation**
Air Density	(kg/m^3)	ρ
Air Velocity (IAS)	Knot	V
Vertical Distance Between Target and Helicopter	Meter	h
Horizontal Distance Between Target and Helicopter	Meter	y
Required Pitch Angle	Degree	θ

Table 3: Sample Data

ρ	**V**	**h**	**θ**	**y**
1.225	0	15.24	1	211.497
1.225	60	243.84	3	5025.307
1.225	120	609.6	10	6749.468

The launcher has a +0 degrees pitch angle with respect to the helicopter body, which is the command pitch angle that the aircraft should have adopted with respect to earth.

2.1 Physical Characteristics of Hydra-70 Rocket

The proposed rocket is called the Hydra-70. It is a 2.75-inch fin-stabilized unguided rocket used on attack helicopters as the air-to-ground weapon system. It can be equipped with a variety of warheads as required for various missions [16]. The physical characteristics of the 2.75-inch rockets with an MK-66 rocket motor are given in Table 4.

Table 4: Mass of Hydra-70 [Dahlke & Batiuk, 1990]

	Warhead	**Motor and Warhead**	
		Live	**Fired**
MK-66 Motor Only	---	6.191	2.9166
MK-66 Motor with PD/M151 High-Explosive Warhead	4.218	10.409	7.135

Charubhun et al. modeled the Hydra-70 in their research [17]. The change of mass with respect to time that was obtained from their research was digitized and remodeled in MATLAB and is charted in Figure 6, below.

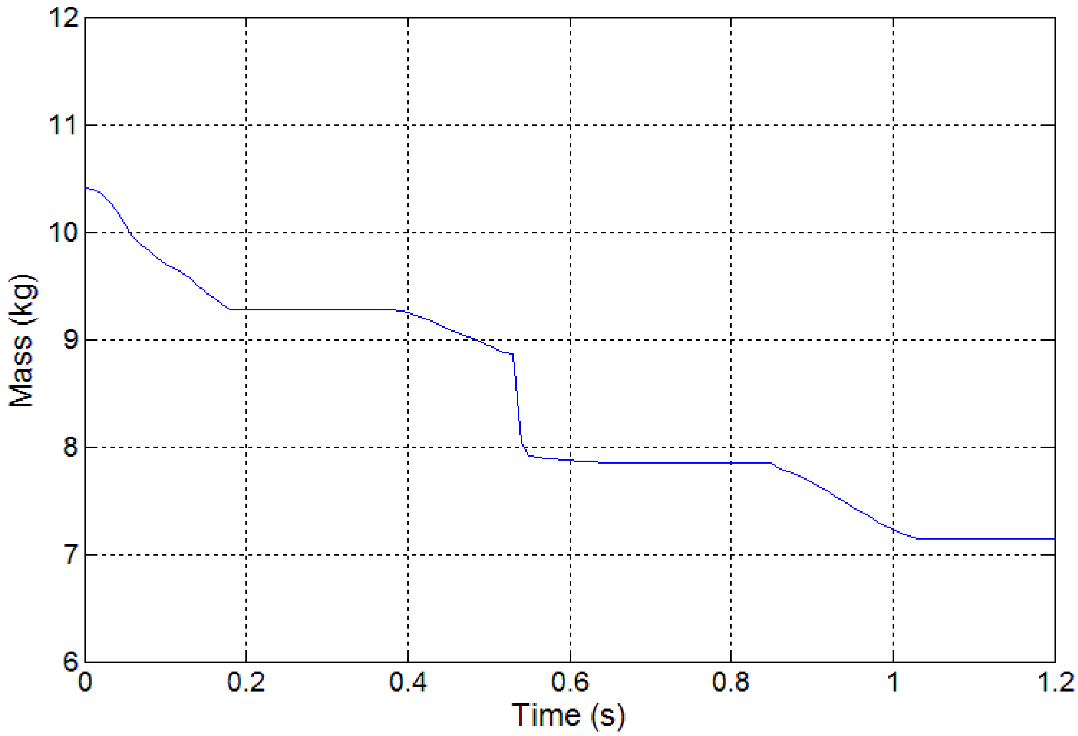

Figure 6: Mass vs. Time

2.2 Rocket Thrust

Given the initial conditions and physical parameters, the trajectory of a rocket's flight was considered to include effects from thrust, drag, change in mass, and gravity.

The drag coefficient, Equation 1, was used as input for the dynamics model, and the drag force of the rocket was estimated using Equation 2 [18].

$$C_d = \frac{F_d}{\frac{1}{2}\rho V^2 A} \tag{1}$$

$$F_d = \frac{1}{2}\rho V^2 C_d A \tag{2}$$

The change in the thrust of the rocket over time that was obtained from the technical report of Dahlke and Batiuk [19], then digitized and remodeled in MATLAB, is shown in Figure 7.

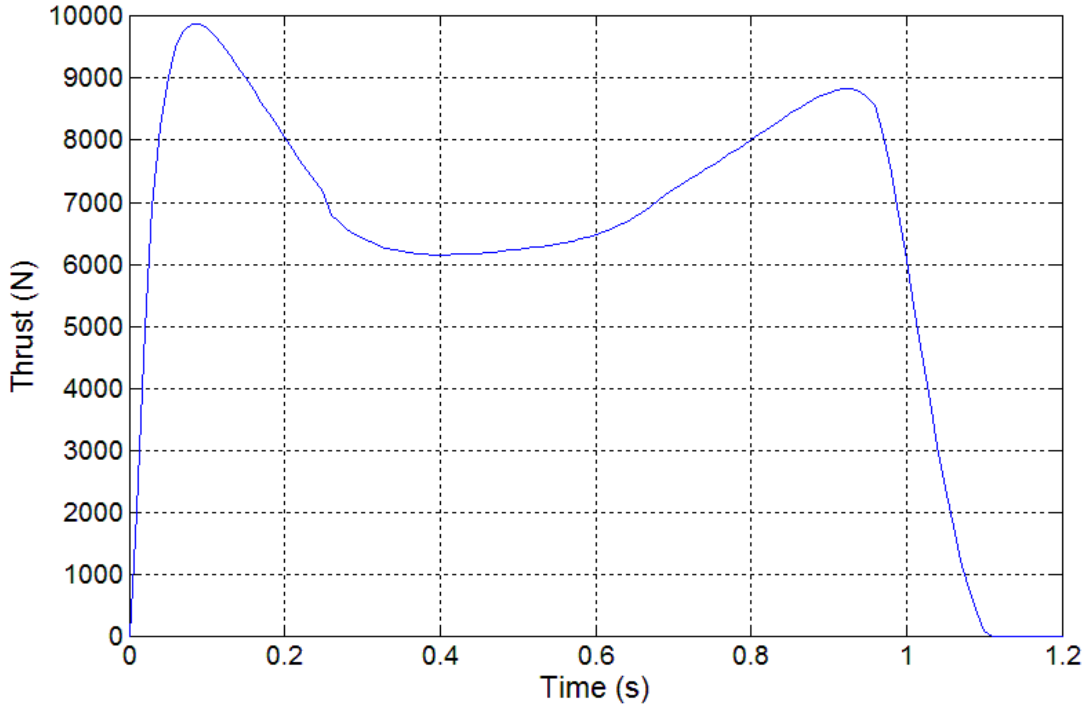

Figure 7: Thrust vs. Time

2.3 The Drag

The drag coefficient for the Hydra-70 was also given in Dahlke and Batiuk [19] for both power-on and coast, with a change in Mach number. The referenced Figure 8 was digitized and recreated in MATLAB and then implemented into the rocket trajectory simulation, which will be explained in next section.

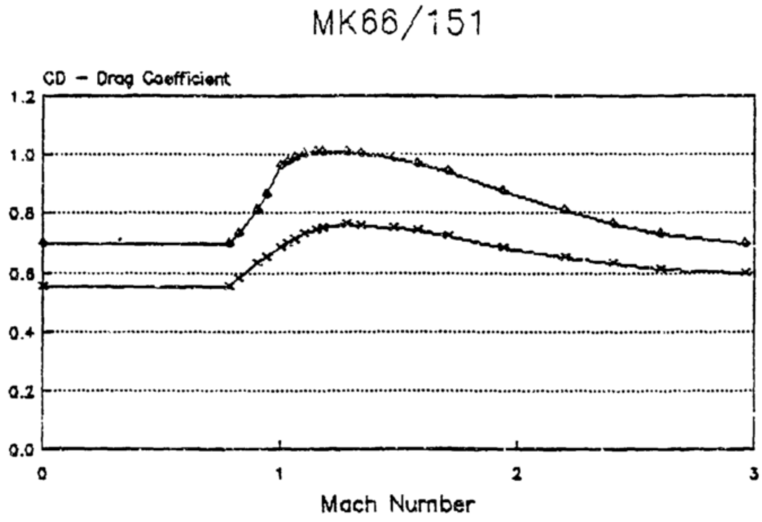

Figure 8: Drag Coefficients [Dahlke and Batiuk, 1990]

2.4 Rocket Trajectory Modeling

Rocket trajectory was calculated using a 2-DOF point mass model in MATLAB. Kapulu has noted that main rotor inflow induces rocket launch. Thus, rocket range extends up to 388 meters for the UH-60 Blackhawk and the Hydra-70 with MK-40 motors [15]. In this study, the inflow of the main rotor was ignored. The trajectory simulation by Parsons was revised and reconstructed for the Hydra-70 introduced in this study [18]. The projected area, initial horizontal speed, and initial vertical speed for the rocket were tuned by hand to adjust the ranges given in rocket delivery charts. Some of the results were compared with rocket delivery charts to validate the model. It was seen that the results were nearly the same. Aerodynamic stability and additional effects such as thrust misalignment that cause dispersion were not taken into consideration. Thus, the actual trajectory in flight can reasonably be expected to not be the same as the estimated trajectory in this study. A sample plot of a rocket trajectory and the dynamics is provided in Figure 9.

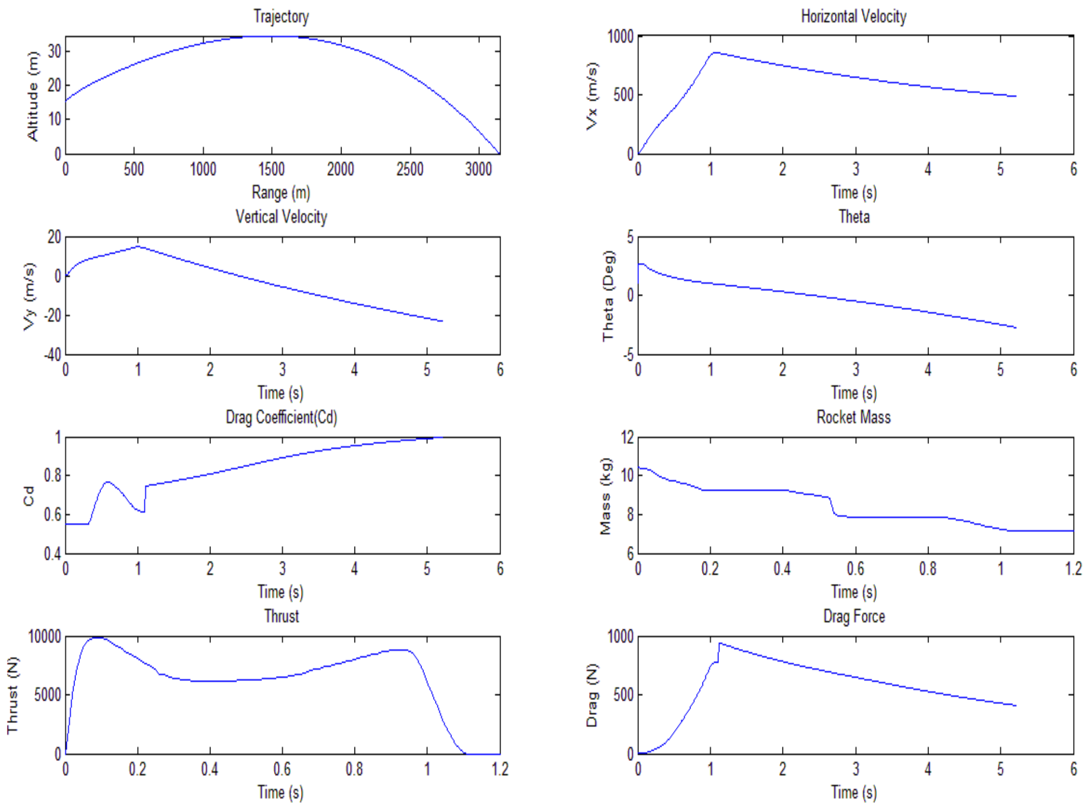

Figure 9: Plots of Rocket Trajectory and Dynamics for ρ=0.885, h=15.24, θ=1,V=0.

2.5 Testing for Normality Using the SPSS 17 Statistics Application

Normality is derived from a normal distribution. The normal distribution shows the shape of data whether or not it is that of a bell curve. The normality of data is a prerequisite for many statistical tests because normal data is an underlying assumption in parametric testing. In many cases, the central limit theorem says that population is approximately normally distributed with a mean of zero and a variance of one when the sample size is greater than 30 [20]. In this study, the sample size was ample, and it is accepted that the data is normally distributed. Also, the histograms of the variables shown in Figure 10 clearly demonstrate a normal distribution. According to George and Mallary [21], it can be said that interested variables are normally distributed if skewness and kurtosis have values between −2 and +2. Table 5 shows that the presented parameters are normally distributed and are convenient for statistical analyses.

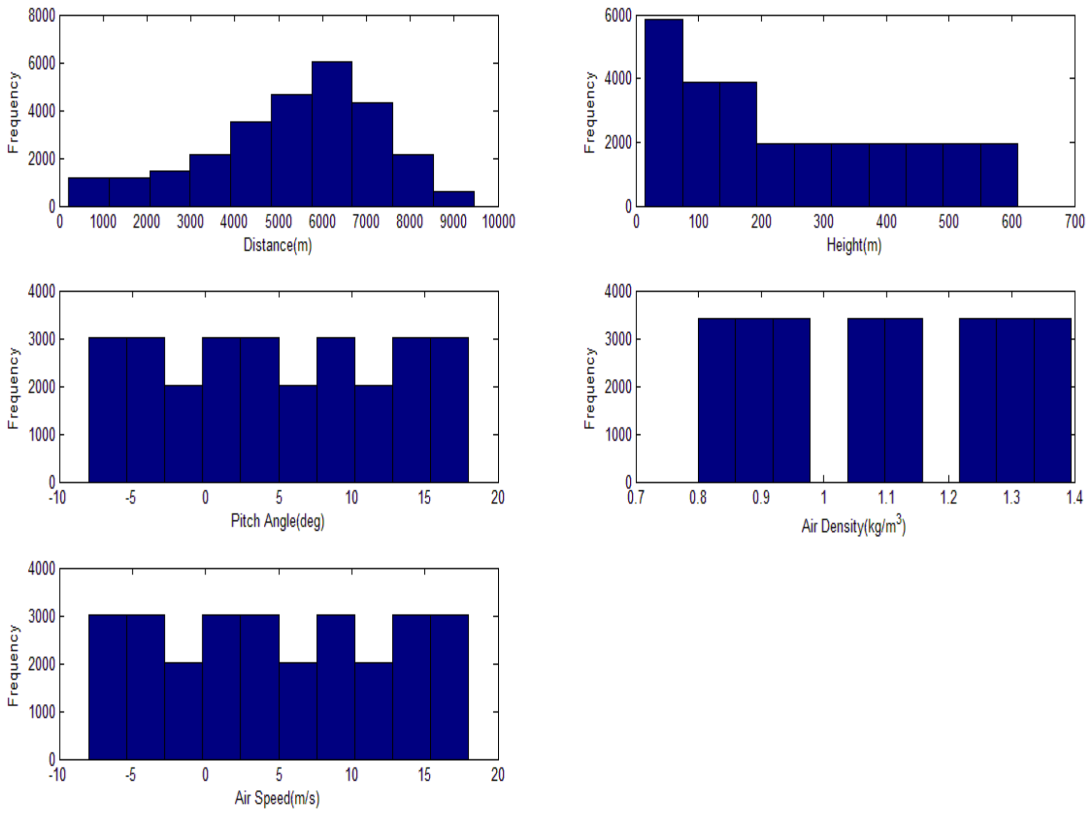

Figure 10: Histograms

Table 5: Skewness and Kurtosis of the Variables

	N	Skewness		Kurtosis	
	Statistic	**Statistic**	**Std. Error**	**Statistic**	**Std. Error**
$\boldsymbol{\rho}$	27216	0.000	0.015	−1.238	0.030
$\boldsymbol{V}$	27216	0.000	0.015	−1.500	0.030
$\boldsymbol{h}$	27216	0.409	0.015	−1.173	0.030
$\boldsymbol{\theta}$	27216	0.000	0.015	−1.203	0.030
$\boldsymbol{y}$	27216	−0.618	0.015	−0.159	0.030
Valid N (list-wise)	27216				

2.6 Correlation Between Variables

Correlation between sets of data refers to a measure of how the variables are related to each other. The most common method for measuring correlation in statistics is the Pearson Correlation, which is also called the Pearson product-moment correlation, or

PPMC. The results provide the correlation of a linear relationship, given as numbers between −1 and 1, for any two data in a data set. It can be said that if the value of a correlation is close to 1, the positive relationship between the two variables is strong, and vice versa [22]. The strength of correlations as described by Pham, [23] are shown below.

- 0.00–0.19 = very weak
- 0.20–0.39 = weak
- 0.40–0.59 = moderate
- 0.60–0.79 = strong
- 0.80–1.0 = very strong

In this thesis, SPSS 17 and MATLAB were the applications used for statistical analyses. The ranges of the estimated data are shown above. All data sets generated by SPSS and output to a table for correlation are shown in Table 6.

Table 6: Correlations Between Variables

		ρ	V	h	θ	y
ρ	Pearson Correlation	1	0.000	0.000	0.000	–0.233**
	Sig. (2-tailed)		1.000	1.000	1.000	0.000
V	Pearson Correlation	0.000	1	0.000	0.000	0.013*
	Sig. (2-tailed)	1.000		1.000	1.000	0.035
h	Pearson Correlation	0.000	0.000	1	0.000	0.383**
	Sig. (2-tailed)	1.000	1.000		1.000	0.000
θ	Pearson Correlation	0.000	0.000	0.000	1	0.835**
	Sig. (2-tailed)	1.000	1.000	1.000		0.000
y	Pearson Correlation	–0.233**	0.013*	0.383**	0.835**	1
	Sig. (2-tailed)	0.000	0.035	0.000	0.000	

** Correlation is significant at the 0.01 level (2-tailed).
* Correlation is significant at the 0.05 level (2-tailed).

If the parameters are correlated with pitch angle, they may be related to each other simply because they are related to the third variable, pitch angle. It may be necessary to know if there are any mutual correlations between parameters that are not due to both variables being correlated with pitch angle. Thus, partial correlations of the parameters, controlled for pitch angle, were calculated using SPSS 17 and are given in Table 7. It is evident that the ongoing model should have mutually correlated terms such as distance with air density, et cetera.

Table 7: Partial Correlations, Controlled for Pitch Angle

Control Variables			ρ	V	h	y
θ	**ρ**	Correlation	1.000	0.000	0.000	–0.423
		Significance (2-tailed)		1.000	1.000	0.000
	V	Correlation	0.000	1.000	0.000	0.023
		Significance (2-tailed)	1.000	.	1.000	0.000
	h	Correlation	0.000	0.000	1.000	0.696
		Significance (2-tailed)	1.000	1.000		0.000
	y	Correlation	–0.423	0.023	0.696	1.000
		Significance (2-tailed)	0.000	0.000	0.000	

In Table 7, it can be seen that there was a strong positive relationship between pitch angle and horizontal distance to target. There was either no correlation or only a weak correlation among the other parameters due to the fact that all models were developed to calculate distance, and all data is set for it. However, as seen in Table 7, if the pitch angle remains constant, mutual correlations occur between range and other parameters. This means that the required pitch angle will be a function of the inputs of air density, air velocity, horizontal distance, and vertical distance. To develop a reliable model with minimum errors, all relationships between variables must be examined and taken into consideration. For example, the multiplication of horizontal distance and vertical distance will be one of the arguments of the function. Curve fitting was applied to construct the mathematical model in MATLAB. While some calculated data fit best to polynomial regression, others fit to Fourier series or linear equations.

2.7 Curve Fitting

Polynomial regression, a form of linear regression, is used to represent and fit nonlinear relationships where the independent variable *x* and the dependent variable *y* are modeled as an *n*th degree polynomial in *x*.

$$y = \beta_0 + \beta_1 x + \beta_2 x^2 + \beta_3 x^3 + \cdots + \beta_n x^n \tag{3}$$

$$\theta = f(\vec{y}; \vec{z}; \vec{V}; \overrightarrow{h}; \vec{T}) + \varepsilon \tag{4}$$

This regression method depends on the choice of degree of the polynomial. First, linear models for each constraint were evaluated, and then the order of polynomials is increased. However, the change of the distance with the pitch angle was a better fit with discrete Fourier transform; the equations obtained are just simple curve fits of sines and cosines.

Curve fitting was used to choose orders of the polynomials. The most common method of curve fitting is the least squares regression analysis, which finds the line of best fit for a data set. Further, nonlinear least squares is a subform of least squares that estimates unknown parameters of a model by successive iterations. The orders are decided where any model of the basic form [19, 21] is

$$y = f(\vec{x}; \vec{\beta}) + \varepsilon. \tag{5}$$

The relationship between pitch angle and other variables were examined, and the model was built in the Curve Fitting function of MATLAB.

2.7.1 Pitch Angle vs. Horizontal Range

To form a relationship between pitch angle and horizontal range, the Fourier fitting method was used. Results are shown in Figure 11 for 1.225 kg/m^3 air density, 50-foot vertical distance, and 60-knot air velocity. A general model for pitch angle and horizontal distance was developed as Fourier Series with R^2=1 and RMSE=0.0653. Equation 6 was applied for other alternatives, and the results are meaningful.

$$\begin{aligned}\theta(y) = a0 \ + \ & a1*cos(y*w)+b1*sin(y*w)+a2*cos(2*y*w) \\ & +b2*sin(2*y*w)+a3*cos(3*y*w)+b3*sin(3*y*w) \\ & +a4*cos(4*y*w)+b4*sin(4*y*w)+a5*cos(5*y*w) \\ & + b5*sin(5*y*w)+a6*cos(6*y*w)+b6*sin(6*y*w)\end{aligned} \tag{6}$$

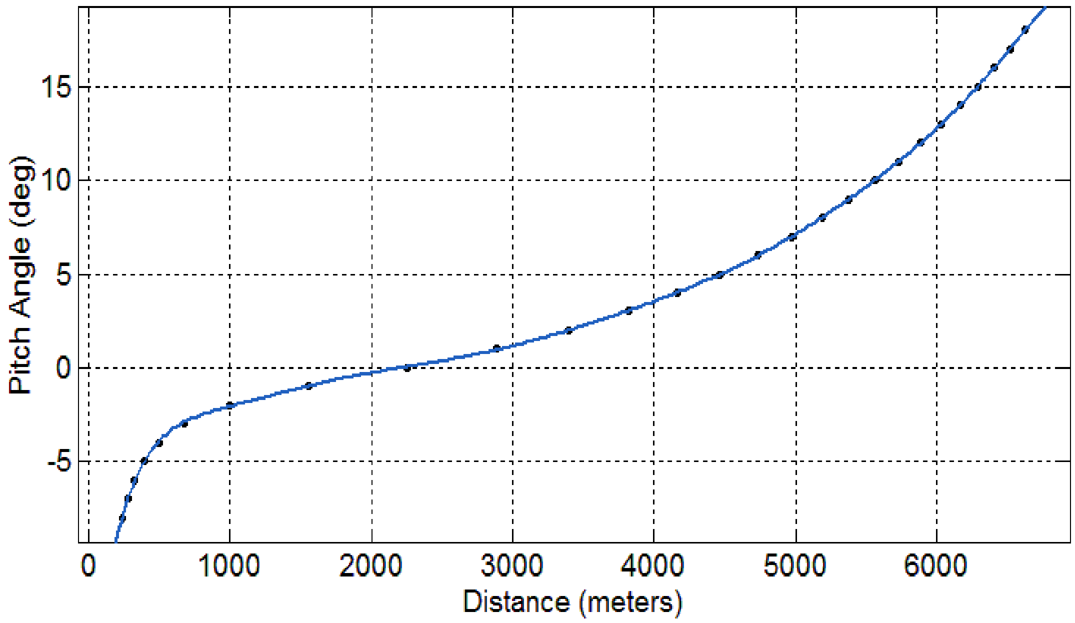

Figure 11: Pitch vs. Horizontal Distance

2.7.2 Pitch Angle vs. Horizontal Distance and Air Density

Dependence of launch angle was derived from the relationship between horizontal distance and air density. Thus, the values were well fitted, and Figure 12 shows the residuals for V=60 knots and h=91.44 m. The pitch angles of θ versus y and ρ were provided as a polynomial in which both were 5th degrees. Thus, the launch angle model becomes a function of ρ and y as a polynomial regression model, with $R^2=1$ and RMSE=0.05176. This is shown below, in Equation 7, where p values are coefficients.

$$
\begin{aligned}
\theta(\rho, y) = {} & p00 + p10*\rho + p01*y + p20*\rho^2 + p11*\rho*y \\
& + p02*y^2 + p30*\rho^3 + p21*\rho^2*y + p12*\rho*y^2 \\
& + p03*y^3 + p40*\rho^4 + p31*\rho^3*y + p22*\rho^2*y^2 \\
& + p13*\rho*y^3 + p04*y^4 + p50*\rho^5 + p41*\rho^4*y \\
& + p32*\rho^3*y^2 + p23*\rho^2*y^3 + p14*\rho*y^4 + p05*y^5
\end{aligned}
\tag{7}
$$

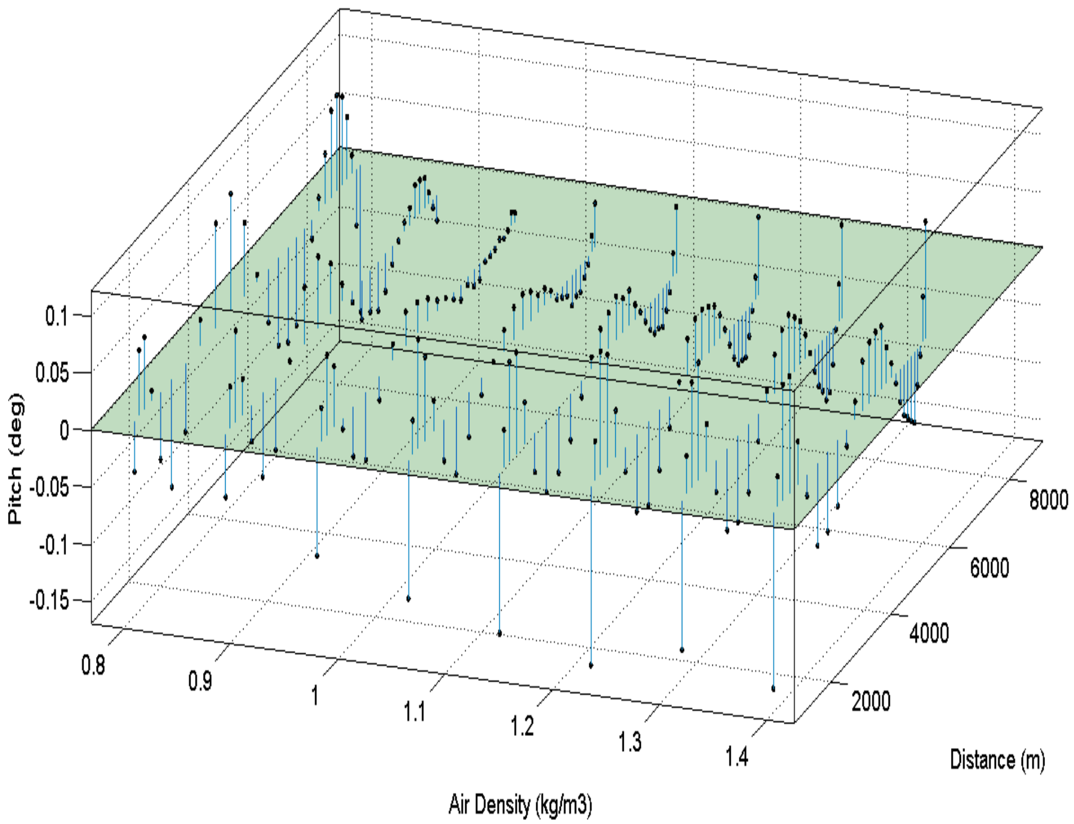

Figure 12: Residuals Plot—Pitch vs. Horizontal Distance and Air Density

2.7.3 Pitch Angle vs. Horizontal Distance and Air Speed

As seen in Table 7, there is an imperceptible correlation of r=0.023 for pitch angle with both velocity and horizontal distance. These two variables affect the required launch angle slightly. However, it is essential to model these parameters to minimize errors in the rocket delivery model. For ρ=1.225 and h=121.92, curve fitting was implemented as a polynomial. The results and the model developed for the required launch angle are shown in Equation 8 and Figure 13, where R^2=1 and RMSE=0.00908.

$$\begin{aligned}\theta(V,y) = {} & p00 + p10*V + p01*y + p20*V^2 + p11*V*y + p02*y^2 \\ & + p21*V^2*y + p12*V*y^2 + p03*V*y^3 + p22*V^2*y^2 \\ & + p13*V*y^3 + p04*y^4 + p23*V^2*y^3 + p14*V*y^4 + p05*y^5\end{aligned} \tag{8}$$

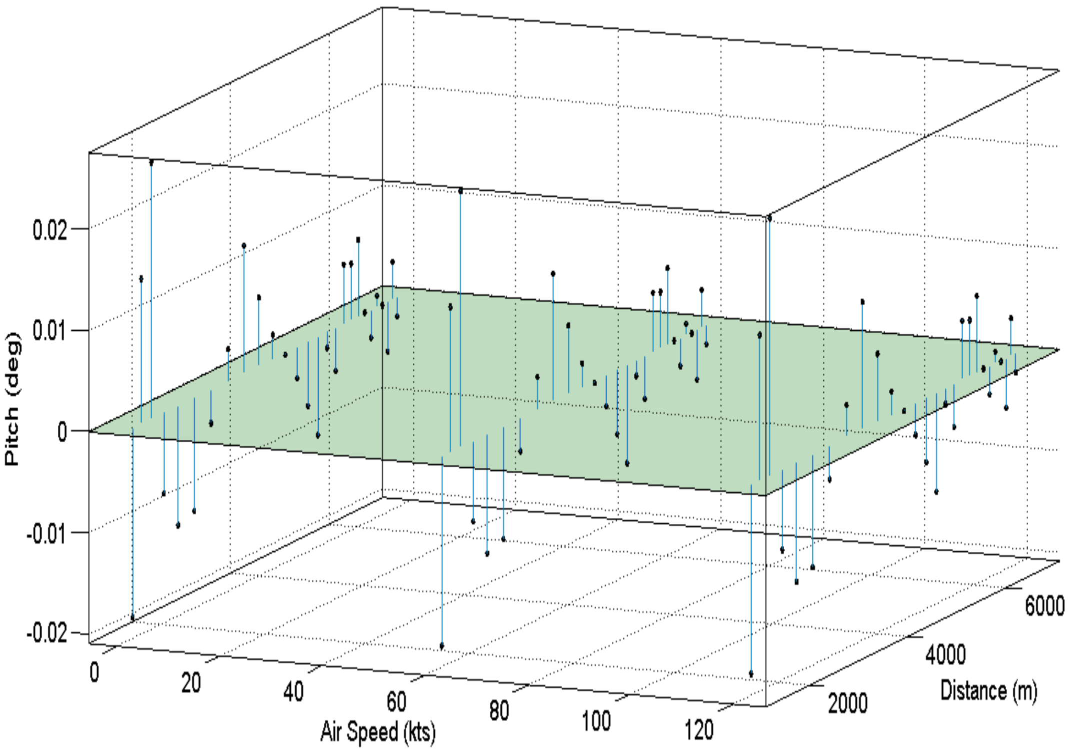

Figure 13: Residuals Plot—Pitch vs. Horizontal Distance and Velocity

2.7.4 Pitch Angle vs. Horizontal and Vertical Distance

Table 7 shows that there was a fair correlation between the control variable of pitch angle and both horizontal and vertical distances from the target, with r=0.696. Note that the model developed here constitutes a major part of the rocket delivery model that is covered in the next section. The model was built for *V*=60 knots and ρ=1.225, and the results are shown in Figure 14 and Equation 9, where R^2=0.9998 and RMSE=0.1066.

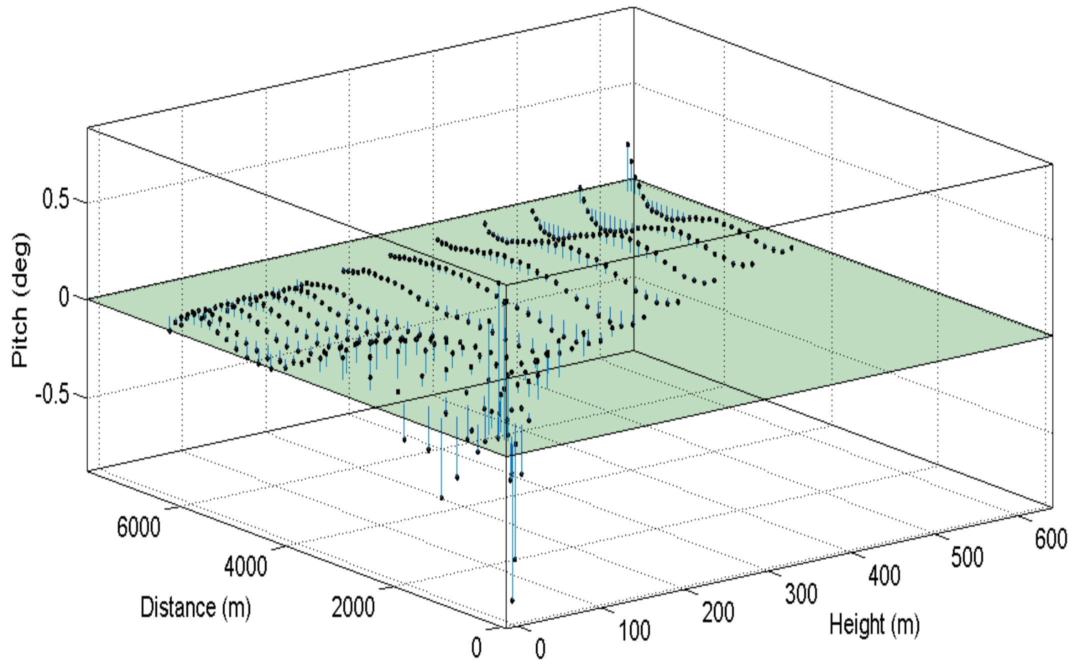

Figure 14: Residuals Plot, Pitch Angle vs. Horizontal, and Vertical Distance

$$
\begin{aligned}
\theta(h, y) = {} & p00 + p10*h + p01*y + p20*h^2 + p11*h*y + p02*y^2 \\
& + p30*h^3 + p21*h^2*y + p12*h*y^2 + p03*y^3 + p40*h^4 \\
& + p31*h^3*y + p22*h^2*y^2 + p13*h*y^3 + p04*y^4 + p50*h^5 \\
& + p41*h^4*y + p32*h^3*y^2 + p23*h^2*y^3 + p14*h*y^4 + p05*y^5
\end{aligned} \tag{9}
$$

2.7.5 The Polynomial Regression Model

To form this model, Equations 6 through 9 were added together and solved in SPSS 17 as a custom regression model [24]. Thus, the function of pitch is as shown in Equation 10, where coefficients are estimated after 50 iterations, shown in Table 8.

$$
\begin{aligned}
\theta(y,h,V,\rho) = {} & C1 + C2*\cos(y*w) + C3*\sin(y*w) + C4*\cos(2*y*w) \\
& + C5*\sin(2*y*w) + C6*\cos(3*y*w) + C7*\sin(3*y*w) \\
& + C8*\cos(4*y*w) + C9*\sin(4*y*w) + C10*\cos(5*y*w) \\
& + C11*\sin(5*y*w) + C12*\cos(6*y*w) + C13*\sin(6*y*w) \\
& + C14*\rho + C15*\rho^2 + C16*\rho*y + C17*\rho^3 + C18*\rho^2*y \\
& + C19*\rho*y^2 + C20*\rho^4 + C21*\rho^3*y + C22*\rho^2*y^2 \\
& + C23*\rho*y^3 + C24*\rho^5 + C25*\rho^4*y + C26*\rho^3*y^2 \\
& + C27*\rho^2*y^3 + C28*\rho*y^4 + C29*V + C30*V^2 \\
& + C31*V*y + C32*V^2*y + C33*V*y^2 + C34*V*y^3 \\
& + C35*V^2*y^2 + C36*V*y^3 + C37*V^2*y^3 + C38*V*y^4 \\
& + C39*h + C40*h^2 + C41*h*y + C42*h^3 + C43*h^2*y \\
& + C44*h*y^2 + C45*h^4 + C46*h^3*y + C47*h^2*y^2 + C48*h*y^3 \\
& + C49*h^5 + C50*h^4*y + C51*h^3*y^2 + C52*h^2*y^3 + C53*h*y^4 + C54*y \\
& + C55*y^2 + C56*y^3 + C57*y^4 + C58*y^5
\end{aligned}
\tag{10}
$$

The estimated model for calculating the required launch angle was run for the entire data set, and the results were compared. The mean absolute deviation of the regression model was e=0.1368, which was caused by residuals in the partial regression models discussed in the previous sections.

Table 8: Estimated Parameters

Coef.	Estimate	Std. Error	95% Confidence Interval		Coef.	Estimate	Std. Error	95% Confidence Interval	
			Lower Bound	Upper Bound				Lower Bound	Upper Bound
C1	−1.88E+01	1.45E+01	−4.71E+01	9.55E+00	**C30**	−5.38E−07	3.60E−06	−7.59E−06	6.51E−06
C2	−4.45E−03	1.32E−03	−7.03E−03	−1.88E−03	**C31**	3.12E−06	4.09E−07	2.32E−06	3.92E−06
C3	4.99E−03	1.31E−03	2.41E−03	7.56E−03	**C32**	4.24E−10	2.88E−09	−5.22E−09	6.07E−09
C4	1.80E−03	1.31E−03	−7.69E−04	4.36E−03	**C33**	−8.22E−10	1.21E−10	−1.06E−09	−5.84E−10
C5	4.10E−03	1.31E−03	1.53E−03	6.67E−03	**C34**	−2.59E−11	4.32E−09	−8.50E−09	8.44E−09
C6	−7.62E−04	1.31E−03	−3.32E−03	1.80E−03	**C35**	−5.46E−14	6.77E−13	−1.38E−12	1.27E−12
C7	5.67E−04	1.31E−03	−2.00E−03	3.13E−03	**C36**	2.60E−11	4.32E−09	−8.44E−09	8.50E−09
C8	−1.28E−03	1.30E−03	−3.83E−03	1.28E−03	**C37**	2.09E−19	4.75E−17	−9.29E−17	9.33E−17
C9	4.50E−04	1.31E−03	−2.13E−03	3.03E−03	**C38**	−1.02E−18	7.57E−19	−2.50E−18	4.67E−19
C10	7.56E−04	1.32E−03	−1.82E−03	3.33E−03	**C39**	−1.50E−01	4.15E−04	−1.51E−01	−1.49E−01
C11	1.05E−03	1.30E−03	−1.50E−03	3.60E−03	**C40**	5.45E−05	3.00E−06	4.86E−05	6.04E−05
C12	−1.11E−03	1.31E−03	−3.68E−03	1.45E−03	**C41**	7.68E−05	3.84E−07	7.60E−05	7.75E−05
C13	9.64E−04	1.31E−03	−1.60E−03	3.53E−03	**C42**	−2.25E−07	8.88E−09	−2.42E−07	−2.08E−07
C14	4.01E+01	6.64E+01	−8.99E+01	1.70E+02	**C43**	3.09E−09	1.16E−09	8.16E−10	5.37E−09
C15	−6.11E+01	1.21E+02	−2.99E+02	1.76E+02	**C44**	−1.82E−08	1.45E−10	−1.85E−08	−1.79E−08
C16	−2.19E−02	4.07E−03	−2.99E−02	−1.40E−02	**C45**	1.97E−10	1.41E−11	1.69E−10	2.24E−10
C17	5.36E+01	1.10E+02	−1.62E+02	2.69E+02	**C46**	3.66E−11	1.39E−12	3.39E−11	3.94E−11
C18	1.15E−02	5.23E−03	1.23E−03	2.17E−02	**C47**	−3.11E−12	2.23E−13	−3.55E−12	−2.68E−12
C19	8.70E−06	2.70E−07	8.17E−06	9.23E−06	**C48**	2.04E−12	2.22E−14	1.99E−12	2.08E−12
C20	−2.57E+01	4.97E+01	−1.23E+02	7.16E+01	**C49**	−7.73E−14	9.23E−15	−9.54E−14	−5.92E−14
C21	−5.62E−04	3.01E−03	−6.46E−03	5.34E−03	**C50**	−1.19E−14	1.02E−15	−1.39E−14	−9.92E−15
C22	−4.39E−06	1.99E−07	−4.78E−06	−4.00E−06	**C51**	−1.76E−15	1.21E−16	−2.00E−15	−1.53E−15
C23	−9.92E−10	1.55E−11	−1.02E−09	−9.62E−10	**C52**	2.51E−16	1.51E−17	2.22E−16	2.81E−16
C24	5.13E+00	8.94E+00	−1.24E+01	2.26E+01	**C53**	−8.63E−17	1.20E−18	−8.86E−17	−8.39E−17
C25	−6.15E−04	6.55E−04	−1.90E−03	6.68E−04	**C54**	2.16E−02	1.20E−03	1.92E−02	2.40E−02
C26	6.47E−07	5.16E−08	5.46E−07	7.49E−07	**C55**	−1.00E−05	1.31E−07	−1.03E−05	−9.74E−06
C27	3.07E−10	4.85E−12	2.98E−10	3.17E−10	**C56**	1.92E−09	1.48E−11	1.89E−09	1.95E−09
C28	3.54E−14	4.52E−16	3.45E−14	3.63E−14	**C57**	−1.69E−13	1.17E−15	−1.71E−13	−1.67E−13
C29	−5.22E−03	4.60E−04	−6.12E−03	−4.32E−03	**C58**	5.74E−18	4.29E−20	5.65E−18	5.82E−18

At closer horizontal distances, the error becomes greater, while there is relatively no error between 3,000 and 5,000 meters. Beyond these distances, the model's error becomes insignificantly greater. Sample data was validated and is presented in Table 9 for randomly produced parameters.

Table 9: The Model Validation

ρ [kg/m³]	V [kts]	h [m]	θ [deg]	y [deg]	Model Est. θ [deg]	Error [deg]
1.304	24.76	113.47	−0.5190	3357.35	−0.5299	0.0109
0.822	12.15	84.38	1.5488	4475.14	1.46109	0.0877
0.838	82.17	63.13	16.7482	8252.85	16.7656	−0.0174
0.814	18.47	45.73	−5.1757	912.89	−5.2253	0.0496
1.275	71.36	40.85	11.2797	5710.53	11.3644	−0.0847
1.345	46.79	24.19	1.0025	2931.97	1.16959	−0.1670
1.103	74.52	97.66	0.0990	3636.33	−0.0006	0.0996
1.008	82.30	79.67	2.7153	4591.29	2.63323	0.0821
1.024	31.02	60.21	6.1137	5429.61	6.15336	−0.0396
1.274	88.46	105.05	−4.1472	2097.42	−4.0993	−0.0479
0.812	57.79	61.52	5.6356	5968.18	5.83286	−0.1972
1.348	119.50	91.02	8.2860	5243.77	8.27343	0.0126
1.069	25.28	54.32	2.8325	4308.20	2.76159	0.0709
1.098	34.68	61.29	13.3513	6573.12	13.4459	−0.0945
0.879	3.34	19.70	14.9690	7636.38	14.979	−0.0100
0.935	78.58	50.64	15.6319	7562.57	15.3738	0.2581
1.151	39.82	79.64	−3.2897	2000.33	−3.1897	−0.1000
1.182	108.66	93.45	13.7545	6446.30	13.7292	0.0252
1.266	77.63	34.65	3.1777	3988.48	3.08588	0.0918
1.295	59.66	51.85	−2.9739	1611.82	−2.8665	−0.1073
1.211	76.04	17.56	−1.6222	1277.53	−1.6002	−0.0220
0.902	45.26	29.76	14.1076	7426.59	14.0371	0.0705
1.098	105.05	91.90	2.0419	4302.88	1.92545	0.1165
0.857	55.93	69.81	5.4347	5794.03	5.65005	−0.2153
1.091	73.76	49.81	−1.0328	2487.16	−0.8715	−0.1613
1.391	10.96	89.14	0.0350	3240.50	0.03574	−0.0008
1.015	115.94	75.45	−2.8929	2143.65	−2.783	−0.1099
0.997	89.27	58.91	−0.9931	2726.29	−0.9244	−0.0687
1.179	66.33	111.31	7.1228	5462.31	7.12517	−0.0024
0.809	12.66	102.58	−5.3240	1735.66	−5.2144	−0.1096
0.865	49.67	64.61	0.4388	3658.01	0.30398	0.1349
1.199	97.37	78.95	1.6085	3915.87	1.49041	0.1181
1.387	100.11	94.86	11.7463	5634.45	11.839	−0.0928
0.813	18.20	81.35	−5.6887	1358.85	−5.6027	−0.0861
1.109	59.90	109.41	8.4440	5882.84	8.52087	−0.0768
0.822	96.24	103.73	11.0214	7457.37	10.9174	0.1041
0.909	14.63	72.22	1.0775	3998.11	0.96529	0.1122
1.085	1.49	18.94	−5.2068	418.65	−5.6599	0.4530
1.267	36.45	41.97	2.5080	3800.09	2.42783	0.0802

CHAPTER 3

LAUNCHER DYNAMIC MODEL

In this chapter, the required dynamic model of the M260 rocket launcher is obtained, and the methods are described.

3.1 Launcher and Rocket Physical Model

The M260 rocket launcher, which is a lightweight aluminum rocket launcher capable of launching all Hydra-70 rockets, is primarily used in attack helicopters. The physical characteristics of the M260 rocket launcher and the rocket are shown in Table 10.

Table 10: Physical Characteristics of the M260 [16,23]

Component	*#*	**M260**	**Rocket**
Mass	*lbs*	35	22.95
Length	*ft*	5.5158	4.59375
Diameter	*ft*	0.8097	0.2296
$\mathbf{x_G}$	*ft*	0	0
$\mathbf{y_G}$	*ft*	0.40485	0.11155
$\mathbf{z_G}$	*ft*	2.86041	2.496
$\mathbf{I_{xx}}$	$slug\text{-}ft^2$	0.123	0.00566
$\mathbf{I_{yy}}$	$slug\text{-}ft^2$	2.63	1.3485
$\mathbf{I_{zz}}$	$slug\text{-}ft^2$	2.64	1.3485

3.2 Active Launcher Mechanism

The so-called active launcher system assumed that a servo motor that was mounted on the geometric center of the launcher controlled the launcher in the y-axis direction as well as up and down by applying torque. The calculated required pitch angle was the control input of the system. The controller applies torque input to the servo to provide an accurate launch angle for the rocket. The active launcher mechanism is demonstrated in Figure 15.

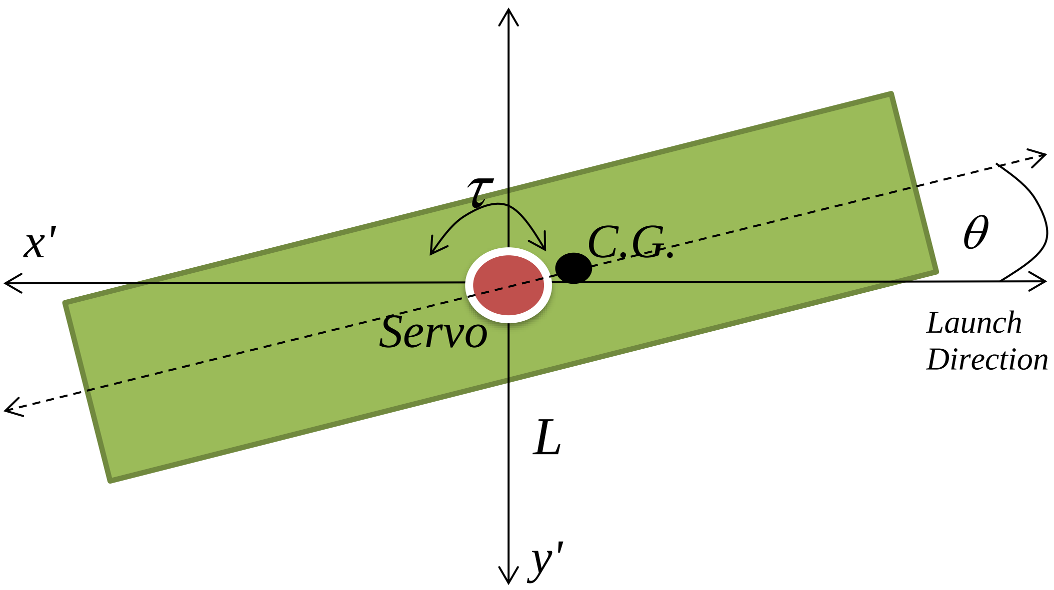

Figure 15: Controlled Launcher Demonstration

3.3 Parallel Axis Theorem

The quantities I_{xx}, I_{yy}, and I_{zz} are the moments of inertia with respect to the x, y, and z axes given in Figure 16, as expressed by Equation 11.

$$I_{xx} = \int_m (y'^2 + z'^2)dm \quad I_{yy} = \int_m (x'^2 + z'^2)dm \quad I_{zz} = \int_m (x'^2 + y'^2)dm \tag{11}$$

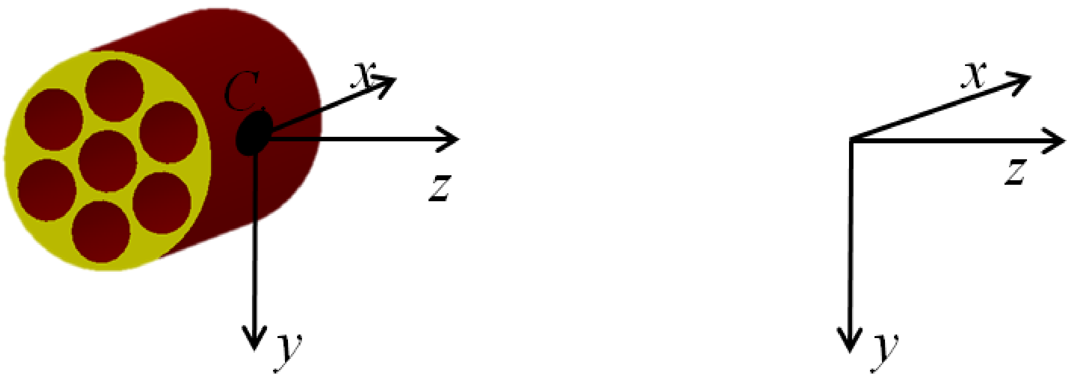

Figure 16: Axis Definition

It was observed that the quantity in the integrand is the square of the distance to the x, y, and z axes and correspond to the moment of inertia used in the two-dimensional case. From their expressions, it can be said that the moments of inertia are always positive. The quantities I_{xy}, I_{xz}, I_{yx}, I_{yz}, I_{zx}, and I_{zy} are called products of inertia. They can be positive, negative, or zero, and are given by Equation 12.

$$I_{xy} = I_{yx} = \int_m x'y'dm \qquad I_{xz} = I_{zx} = \int_m x'z'dm \qquad I_{yz} = I_{zy} = \int_m y'z'dm \tag{12}$$

The moments of products of inertia have expressions that are related to those given above, but x', y', and z' are replaced by x, y, and z.

$$(I_{xx})_O = \int_m (x^2 + y^2)dm \qquad (I_{yy})_O = \int_m (x^2 + z^2)dm \qquad (I_{zz})_O = \int_m (x^2 + y^2)dm \; , \tag{13}$$

and

$$(I_{xy})_O = (I_{yx})_O = \int_m (xy)dm \; (I_{xz})_O = (I_{zx})_O = \int_m (xy)dm \;\; (I_{yz})_O = (I_{zy})_O = \int_m (yz)dm \tag{14}$$

If the moment of inertia of an object about an axis of rotation that passes through its center of mass is known, then the moment of inertia of this object about any axis parallel to this axis can be found using Equation 15.

$$(I_{xx})_o = \int_m (y^2+z^2)dm = \int_m ((y_G+y')+(z_G+z')^2)dm$$
$$= \int_m (y'^2+z'^2)+2y_G\int_m (y'dm+2z_G\int_m z'dm+(y_G^2+z_G^2)\int_m dm$$
$$= I_{xx}+m(y_G^2+z_G^2) \tag{15}$$

Here, we have used the fact that y' and z' are the coordinates relative to the center of mass, and therefore, their integrals over the body are equal to zero. Similarly, we can now write out Equations 16 through 20.

$$(I_{yy})_O = I_{yy}+m(x_G^2+z_G^2) \tag{16}$$

$$(I_{zz})_O = I_{zz}+m(x_G^2+y_G^2) \tag{17}$$

$$(I_{xy})_O = (I_{yx})_O = I_{xy}+mx_G y_G \tag{18}$$

$$(I_{xz})_O = (I_{zx})_O = I_{xz}+mx_G z_G \tag{19}$$

$$(I_{yz})_O = (I_{zy})_O = I_{yz}+my_G z_G \tag{20}$$

3.4 Center of Gravity, Mass, and Inertia

The number of rockets fired is the pilot’s choice because, in tactical situations, pilots can fire one to seven rockets from one launcher at the same time. In this study, rockets were fired one by one, and estimations were calculated in that respect. The rocket and launcher models were developed in the CATIA environment, as shown in Figure 17. The warhead and the rocket motor were assumed to be and modeled as a cylinder. The individual physical characteristics of the rocket and the launcher were already presented in Table 10. Using these parameters, the mass, inertia, and center of gravity values were calculated together and separately for each situation in which the rocket fired in the order shown in Figure 18.

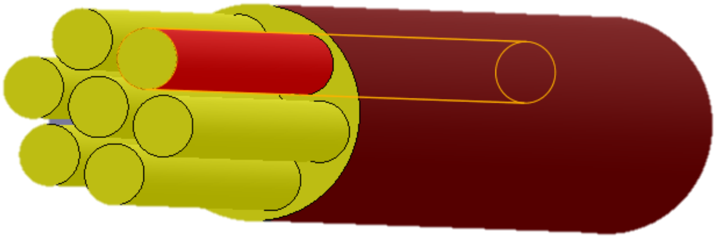

Figure 17: Front View of CATIA Model

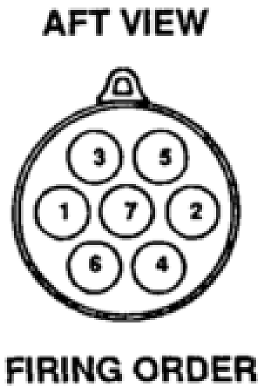

Figure 18: Firing Order as Given

As expected, for each firing session, the dynamics changed. For each case, the center of gravity was estimated in the CATIA environment. Origin of the reference coordinate system was at the front side zero line of the launcher. Then, the parallel axis theorem, presented in Section 3.2, was used to calculate the inertias. The results are shown in Table 11.

Table 11: Center of Gravity, Mass, and Inertia Values

Component #	x_G [m]	y_G [m]	z_G [m]	I_{xx} [kg*m^2]	I_{yy} [kg*m^2]	I_{zz} [kg*m^2]	mass [kg]
FULL	0.0000	0.1229	0.5008	92.1482	108.1109	28.7997	88.745
Rocket 1 Fired	−0.0105	0.1229	0.5115	89.6614	101.4206	24.5884	78.3354
Rocket 2 Fired	0.0000	0.1228	0.5256	86.4148	94.5298	20.9361	67.9254
Rocket 3 Fired	−0.0068	0.1353	0.5447	80.1171	87.7247	16.6641	57.5155
Rocket 4 Fired	0.0000	0.1230	0.5723	72.4764	79.1435	13.1719	47.1055
Rocket 5 Fired	0.0107	0.1426	0.6154	60.4478	66.7308	8.6786	36.6956
Rocket 6 Fired	0.0000	0.1234	0.6929	41.4730	46.6927	5.4076	26.2856
Rocket 7 Fired	0.0000	0.1234	0.8718	0.16677	3.56580	3.5793	15.8757

3.5 Dynamic Modeling

The course change was measured in degrees as θ. As can be seen in Figure 18, at full rocket load, the center of gravity was in front of the mount point, as λ. Alternative approaches for controlling the launcher may have also been developed.

3.5.1 Equation of Motion

In this model, the second-order effects are summed in one torque equation, and angular acceleration is calculated. Equation of motion is given below.

$$I'_{xx}\ddot{\theta} = -m'g'L'\lambda\sin(\theta) + \tau - b\dot{\theta} \tag{21}$$

Assumptions include $\sin(\theta) = \theta$, and as a result, the equation becomes as shown in Equation 22.

$$I'_{xx}\ddot{\theta} = -m'g'L'\theta + \tau - b\dot{\theta} \tag{22}$$

3.5.2 Open Loop Launcher Model

From the motion equation, uncontrolled transfer functions are obtained for seven firing conditions. The damping ratio of the servo motor was assumed as *b*=300 Ns/m. Thus, the transfer functions between pitch rate of the launcher and the torque applied become as shown in Equations 23 through 29.

Full rocket load : $$\frac{\theta}{\tau} = \frac{1}{92.1482s^2 + 300s + 436.0309} \quad (23)$$

Six-rocket load : $$\frac{\theta}{\tau} = \frac{1}{89.6615s^2 + 300s + 393.1384} \quad (24)$$

Five-rocket load : $$\frac{\theta}{\tau} = \frac{1}{86.4148s^2 + 300s + 350.2458} \quad (25)$$

Four-rocket load : $$\frac{\theta}{\tau} = \frac{1}{80.1172s^2 + 300s + 307.3533} \quad (26)$$

Three-rocket load: $$\frac{\theta}{\tau} = \frac{1}{72.4764s^2 + 300s + 264.4607} \quad (27)$$

Two-rocket load : $$\frac{\theta}{\tau} = \frac{1}{60.4478s^2 + 300s + 221.5683} \quad (28)$$

One-rocket load : $$\frac{\theta}{\tau} = \frac{1}{41.4730s^2 + 300s + 178.6757} \quad (29)$$

3.6 Background on Controller

As mentioned in Section 1.3, an active rocket launcher was controlled by using a PID controller, and the performance of the system was examined under different combat scenarios. First, the controller will be briefly introduced.

3.6.1 Proportional–Integral–Derivative Controller

With its simple structure and its general control algorithm, the PID controller is one of the most commonly used controllers for studies and practical use in this field. Its functional simplicity allows engineers to operate them in a simple and straightforward manner.

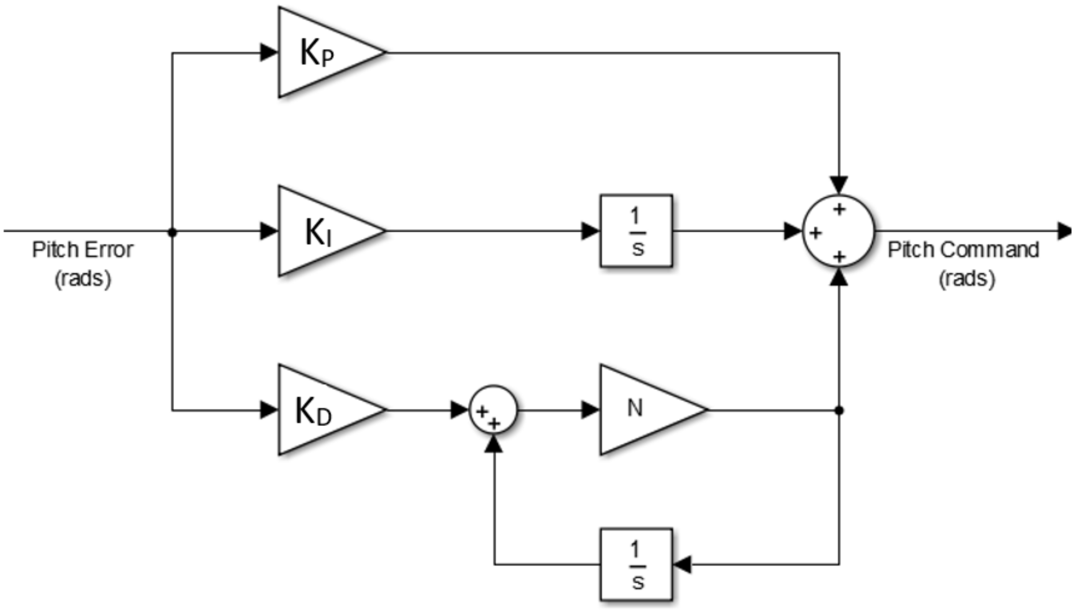

Figure 19: PID Controller Block Diagram

A basic representation of a PID controller is given in Figure 19. The controller takes the amount of error in the control parameters (θ in our case) and applies input to the system according to those parameters, which for this control were K_P=proportional constant, K_D=derivative constant, and K_I=integral constant. The effects of these parameters on the main system response are given in Table 12.

Table 12: The Effects of Each Controller Parameter

Response	Rise Time	Overshoot	Settling Time	S-S Error
K_P	Decrease	Increase	NT	Decrease
K_I	Decrease	Increase	Increase	Eliminates
K_D	NT	Decrease	Decrease	NT

The PID control algorithm is described as;

$$u(t) = K_P e(t) + K_D \frac{de(t)}{dt} + K_I \int e(\Gamma) d\Gamma \qquad (30)$$

3.6.2 Proportional Control

The control action is directly proportional to the error of the controlled signal. In the case of proportional control, it simplifies to Equation 31.

$$u(t) = K_P e(t) + u_b \tag{31}$$

3.6.3 Integral Control

In general, the proportional control leaves a steady-state error, which the integral control removes. The P_I control is shown in Equation 32.

$$u(t) = K_P e(t) + K_I \int e(\Gamma) d\Gamma \tag{32}$$

3.6.4 Derivative Control

Derivative control improves the closed-loop stabilization performance of the controller. The derivative action in the K_D controller essentially responds to the rate of change in the controlled state. The K_D control is shown in Equation 33.

$$u(t) = K_P e(t) + K_D \frac{de(t)}{dt} \tag{33}$$

The derivative control has a high gain for high-frequency changes. Thus, significant changes in the control output occur due to increased noise. In a simulation environment, derivative action without filtering is not necessary because the amplitude of noise is relatively small. However, in actual use experiments, without this filter, the amplitude noise has a significant effect on derivative control that causes the system to become uncontrollable [27].

3.7 Controller Design

To make a stable pitch hold system for the launcher, the response has to be sufficiently quick and robust to helicopter attitude changes. As an initial design, a PID controller structure was chosen, and the gains were calculated with a pole placement method. The following requirements must be determined for the design of the launcher controller.

- Rise Time : 1 s
- Settling Time: 1.5 s
- Overshoot: 1%

With respect to the requirements, PID controller gains were calculated with an N=40 derivative filter using a pole placement method. First, the desired response of the system was determined. Then the system was adjusted to match the desired response. The steps of the applied method are explained below.

- Step 1: Enter the design criteria into the formulas in Equations 34 and 35, below. Then, calculate the natural frequency and damping ratio.

$$\zeta = \frac{-\ln(\%OS/100)}{\sqrt{\pi^2 + \ln^2(\%OS/100)}} \tag{34}$$

$$\omega_n \approx \frac{4}{\zeta T_s} \tag{35}$$

- Step 2: The poles of the closed-loop characteristic equation were determined using Equation 36.

$$\Delta = s^2 + 2\zeta\omega_n s + \omega_n{}^2 \tag{36}$$

- Step 3: Add a root to the real axis by using 50% of the original roots.

- Step 4: Compensate the closed-loop transfer function by using Equation 37 where α is the derivative filter.

$$H = K_P + \frac{\alpha K_D s}{s+\alpha} + \frac{K_I}{s}$$
$$C.L.T.F = \frac{HG}{1+HG} \tag{37}$$

- Step 5: Solve the closed-loop transfer function and desired characteristic equation mutually to find the gains.

The results for this study are given in Table 13.

Table 13: Calculated PID Gains

	Ts=1.5 sn		
	K_P	**K_I**	**K_D**
Full	3259.7	7286.6	469.1
Rocket 1 Fired	3211.8	7107.4	450.19
Rocket 2 Fired	3163.9	6928.2	431.28
Rocket 3 Fired	3025.2	6569.9	393.45
Rocket 4 Fired	2825.8	6092.1	343.02
Rocket 5 Fired	2504.3	5375.4	267.37
Rocket 6 Fired	1971.8	4240.6	147.59

The root locus plot for the fully loaded launcher is represented below in Figure 20. All poles are zeros in LHP, meaning the system is stable.

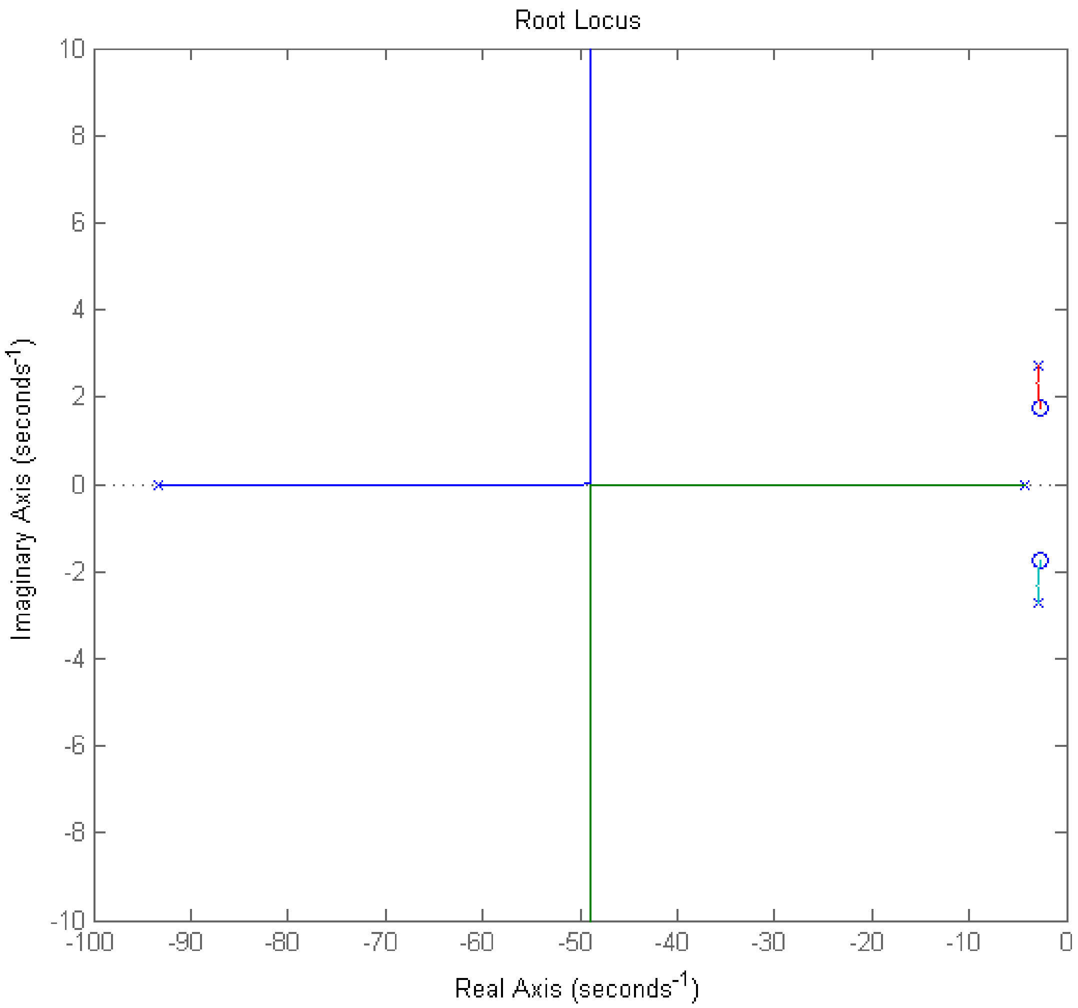

Figure 20: Root Locus Plot of the Fully Loaded System

The 1-degree step response of the fully loaded system is shown in Figure 21. The responses of the other systems were as expected.

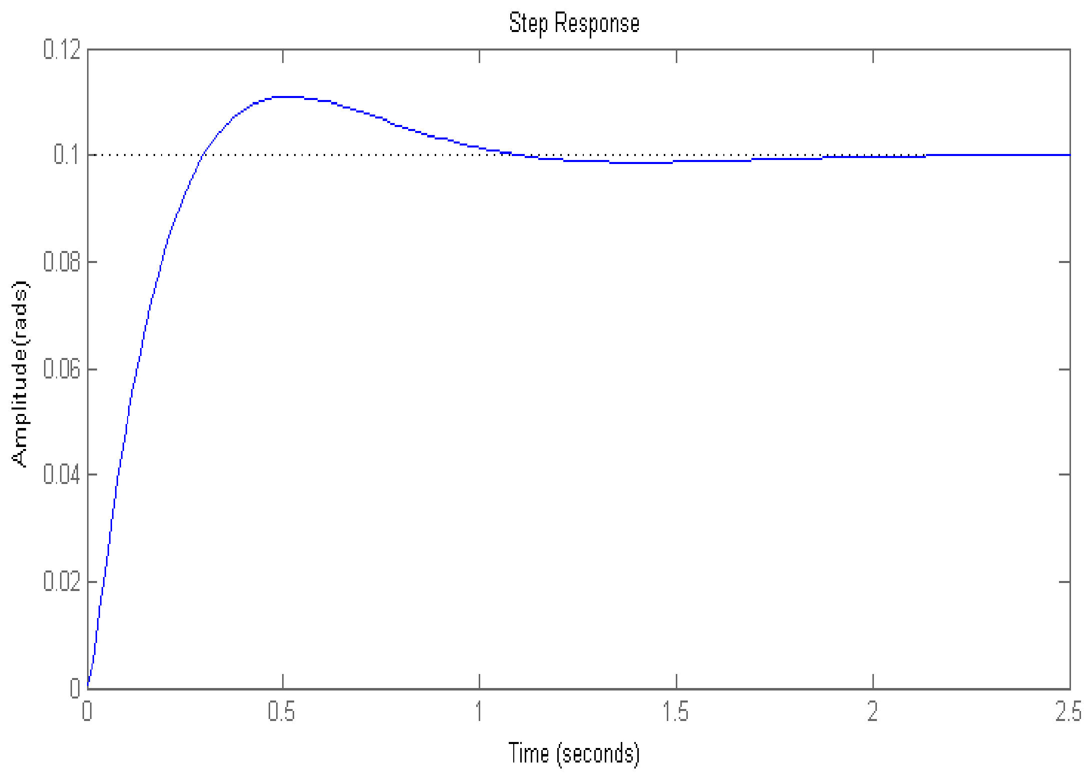

Figure 21: Step Response of the Fully Loaded System

The block diagram of the controller used in the simulation is given in Figures 22 and 23; all seven potential situations for the launcher were built with IF blocks. The SIMULINK checks the remaining rockets and chooses the necessary block for the simulation.

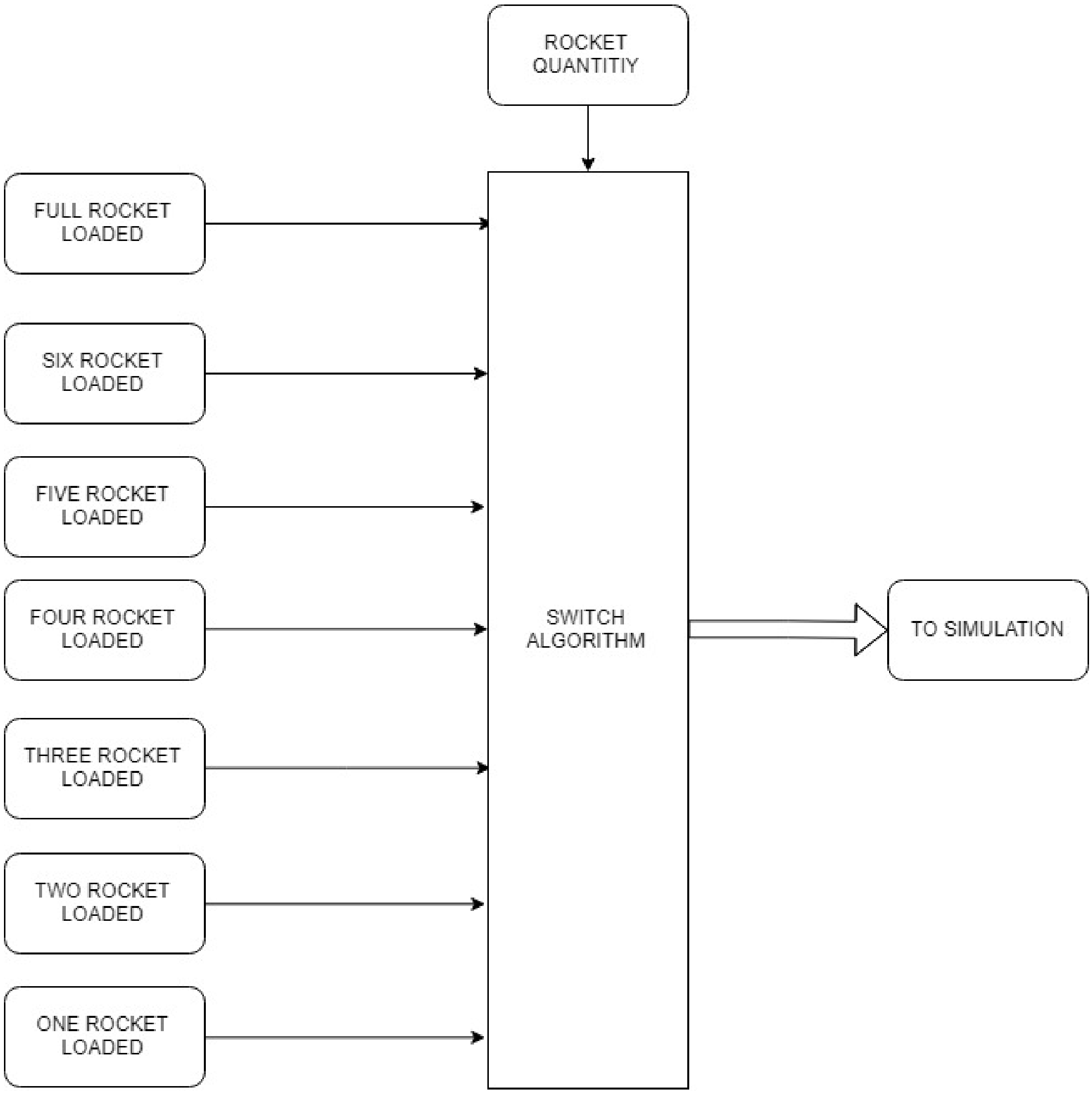

Figure 22: Rocket Load Scenarios Block Diagram

Inside of the block, there is a single block diagram of the closed-loop active launcher system, given in Figure 23.

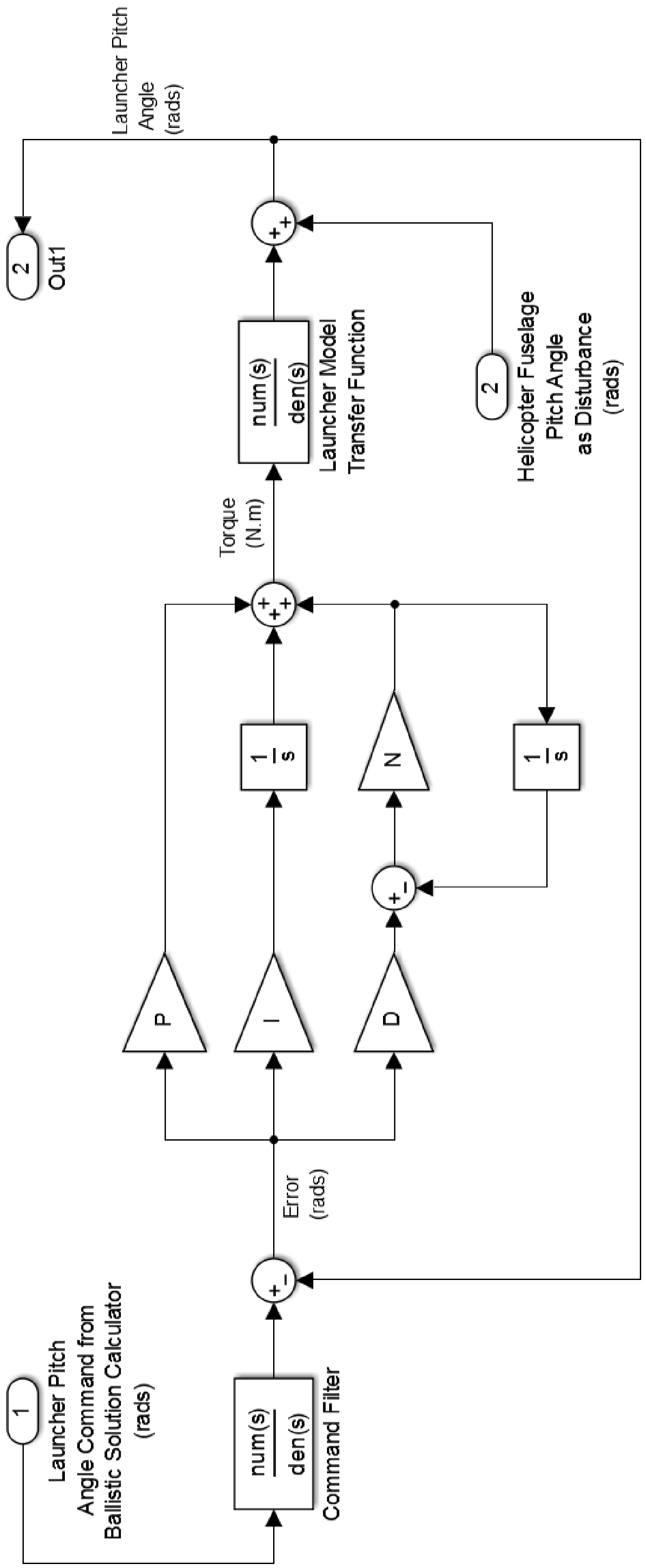

Figure 23: Closed Loop Active Launcher System

CHAPTER 4

THE SIMULATION TESTS

For this study, a PID controller was designed in MATLAB using the requirements as outlined previously. To test the performance of the controller, an active rocket launcher and PID controller were embedded in the UH-1H Helicopter Simulator that was developed in the Simulation, Control, and Avionics Lab of the Department of Aerospace Engineering, METU, by Yılmaz and Yavrucuk [28].

4.1 The Simulation Setup

The simulation was run on MATLAB and SIMULINK with an XPLANE visual environment with a cyclic, collective, and pedals. The knobs on the collective were used to give the target parameters during flight. The block diagram of the Simulation contains the joystick inputs given in Figure 24.

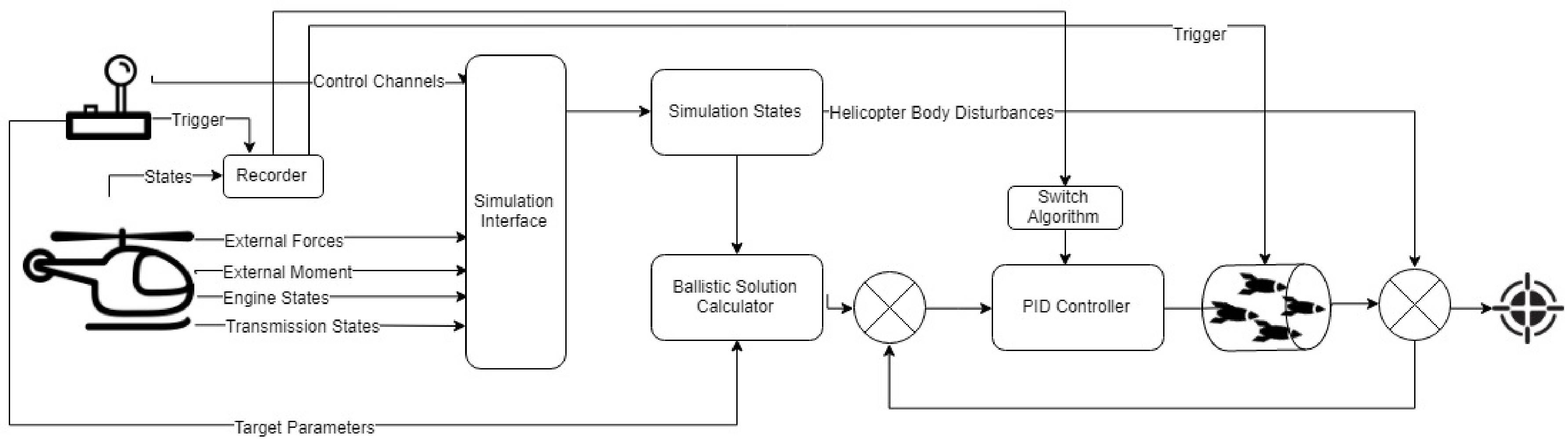

Figure 24: Part of the Simulation Block Diagram

The block diagram of the proposed launcher is shown in Figure 25. The ballistic solution calculator (BSC) takes attitude data from the air data computer and receives target data from cockpit control unit. With this data, the BSC recalculates the reference control value using the previously outlined regression model.

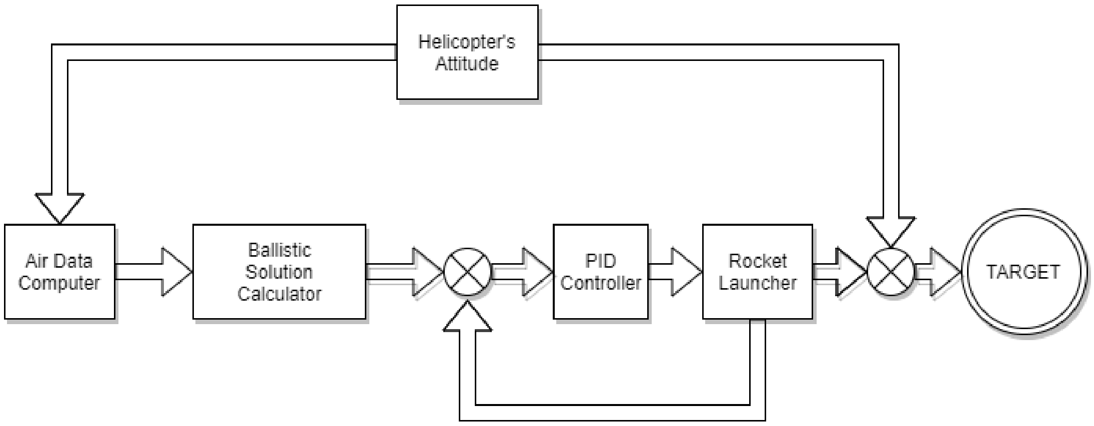

Figure 25: The Block Diagram of the Proposed Launcher System

When the pilot hit the fire button, the simulator recorded the states at that moment. If the rockets hit the target in a 50 x 50 meter square, it was recorded as HIT. Otherwise, it was accepted as MISS. The recording block is shown in Figure 26, and the recorded states were as follows.

- Hit or miss
- Helicopter’s pitch angle
- Launcher’s pitch angle
- Reference pitch angle
- Distance to target
- Height over target
- Temperature
- Altitude
- IAS
- Azimuth angle

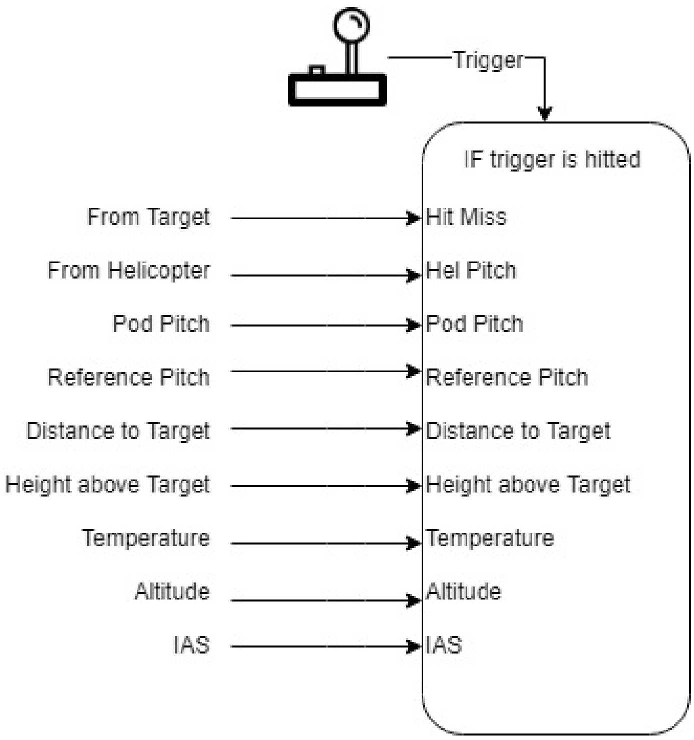

Figure 26: The Recording Block

The BSC took the states and gave commands to the "rocket pods scenarios" block as mentioned above. The reference control input had a limited range of −15 to +15 degrees. The block diagram of this process is shown in Figure 27.

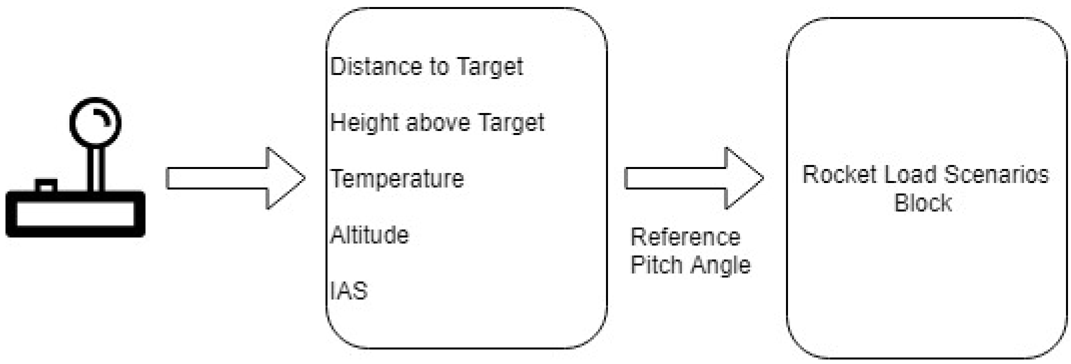

Figure 27: Block Diagram of the Ballistic Solution Calculator

Photos of the setup are presented in Figures 28 through 31. In the first photo, the white window that can be seen displays information about target parameters and the launcher position.

Figure 28: Photo Taken During the Simulation Flight


Figure 29: Photo of the Simulation Setup

Figure 30: Photo of the Simulation Setup

Figure 31: Photo of the Simulation Setup

4.2 The Simulation Results

In the simulated flight, 471 rockets were fired at zero degrees pitch-up fixed launcher, and 611 rockets were fired by the active launcher using both single firing and rapid firing, which seven rockets were fired in a rapid sequence.

With the collected data, the proposed active launcher's performance was tested and compared for the required distances both down-range and cross-range. All results were obtained by flight simulation, and no Monte-Carlo simulation was used in any of the steps. Scenarios were defined to simulate real combat situations taken from the first author's attack helicopter experiences and his colleagues' feedback from the combat zone. Target parameters were input in real time during the simulated flight by using knobs on the joysticks.

A sequence of the simulation is given below in Figure 32. The helicopter's changing attitude generated disturbance on the controller. It is apparently seen that the controlled launcher followed the command irrespective of any changes in the helicopter's pitch angle although minor disturbances occurred due to the different pitch angles. Hence, the launcher was largely unaffected by changing conditions of the aircraft. The step changes in the figure are the reactions of the launcher to new target conditions.

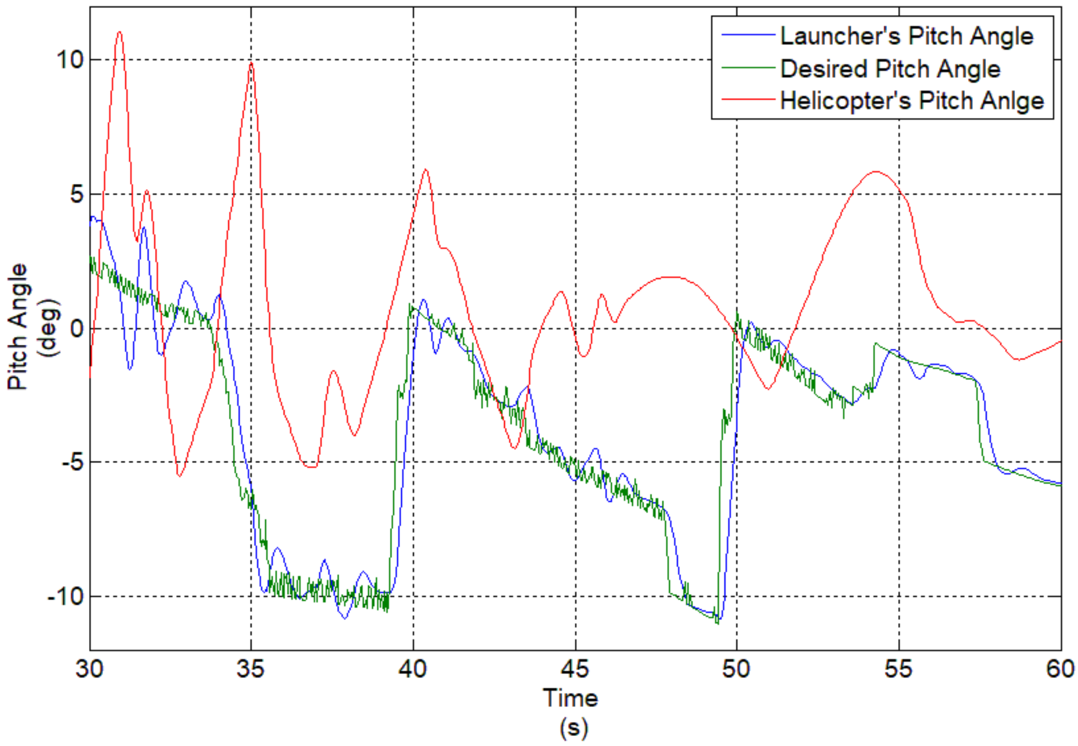

Figure 32: Sequence of the Simulation

It can be seen that the launcher followed the reference input with very little error. Thus, the pilot did not need to provide input for varying target parameters during the flight. The torque applied to the servo is given in Figure 33. The torque varied between −200 to 200 N.m. to change pitch angle of the full loaded rocket launcher. Thus, a minimum 200 N.m capable servo motor will be needed for future design.

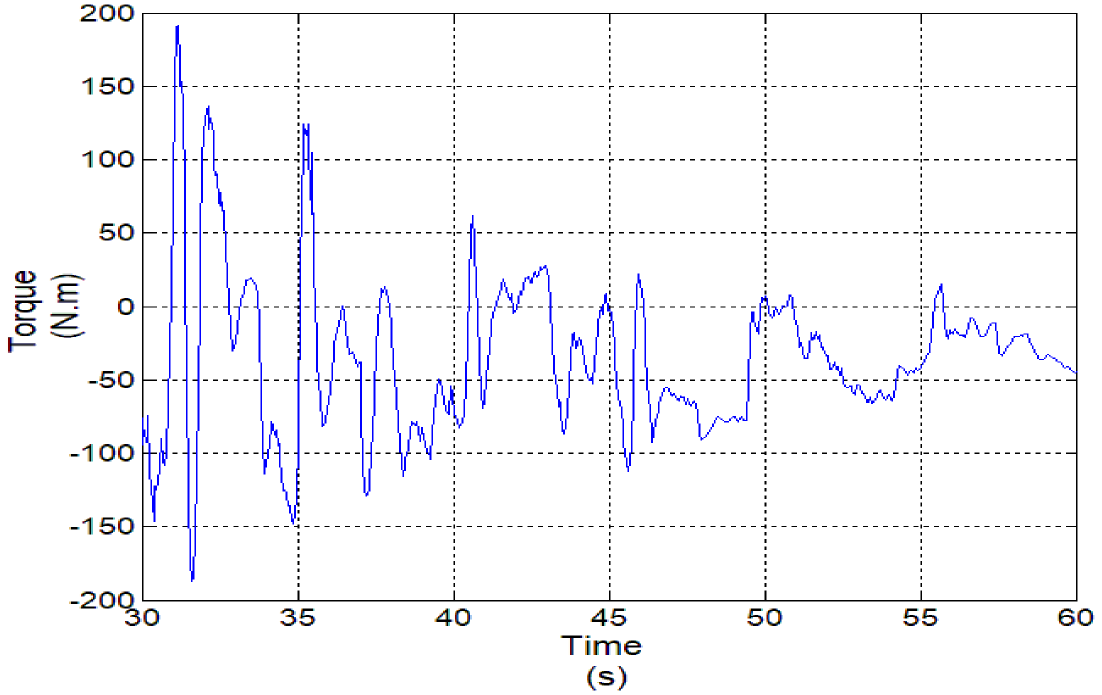

Figure 33: Torque Applied

Sample simulation results of both a fixed and an active launcher are presented below in Table 14. Errors of the fixed and active launchers were compared to examine the performance of the designed system.

Table 14: Sample Record of Rocket Firing Simulation Results

	Helicopter				Target		Launcher			Error	
	Pitch [deg]	**Altitude [ft]**	**OAT [ºC]**	**Velocity [kts]**	**Distance [m]**	**Height [ft]**	**Reference [deg]**	**Output [deg]**	**Hit Dist. [m]**	**Angle [deg]**	**Distance [m]**
Fixed	7.25	2169	10	57	6362	−451	6.29	7.25	5415	0.96	947
	4.57	4886	10	72	7037	520	3.94	4.57	6712	0.63	326
	0.3	4667	10	78	6284	1333	−0.04	0.3	6145	0.34	139
	−5.35	3339	10	58	4680	1751	−5.05	−5.35	4775	−0.3	−95
	−14.44	2622	10	101	1464	796	−12.05	−14.44	1920	−2.39	−457
	−2.03	1228	10	91	3328	592	−3.28	−2.03	2904	1.25	424
	−6.01	5467	10	90	3451	1101	−5.91	−6.01	3478	−0.1	−28
	1.75	2304	10	59	7594	1192	4.18	1.75	8333	−2.43	−739
Active	0.02	2165	−10	53	6205	546	9.21	9.28	6264	−0.07	−58
	−2.50	4432	−10	78	1457	1432	−12.92	−12.88	1439	−0.04	18
	−4.00	4553	−10	81	3362	1553	−2.37	−2.35	3364	−0.02	−2
	−1.08	1463	−10	41	6336	192	10.78	10.75	6342	0.03	−6
	0.23	1881	−10	41	4567	134	8.16	8.17	4525	−0.01	42
	−4.34	4984	−10	88	5059	698	5.84	5.76	4997	0.08	62
	−3.99	6187	−10	87	3842	393	4.93	4.95	3831	−0.02	11
	−0.07	1365	20	70	7026	94	11.48	11.47	7046	0.01	−20
	−4.49	3195	−10	75	2215	575	−0.12	−0.04	2266	−0.08	−51

4.2.1 The Active Launcher

For the active launcher, there was no statistically significant correlation between errors and any variables except for reference pitch angle and horizontal distance. This indicates that increases or decreases in these variables do not significantly relate to increases or decreases in errors. Furthermore, there was minimal correlation between error and the reference pitch angle, at 0.214. Overall results show that errors occurred due to pilot commands. The SPSS output for correlations is given in Table 15.

Table 15: Error Correlations of the Active Launcher

Correlations								
		Hel. Pitch Angle	**Reference Pitch Angle**	**Horz. Dist.**	**Vert. Dist.**	**Alt.**	**IAS**	**# of Fired**
Error	**Pearson Correlation**	−0.016	0.214**	0.100*	−0.066	−0.023	0.014	0.025
	Sig. (2-tailed)	0.689	0.000	0.013	0.104	0.573	0.731	0.533
	N	611	611	611	611	611	611	611
** Correlation is significant at the 0.01 level (2-tailed).								
* Correlation is significant at the 0.05 level (2-tailed).								

The hit positions of the rockets were standardized and scaled to zero–zero coordinates to demonstrate the rocket dispersions for each firing, which is shown in Figure 34.

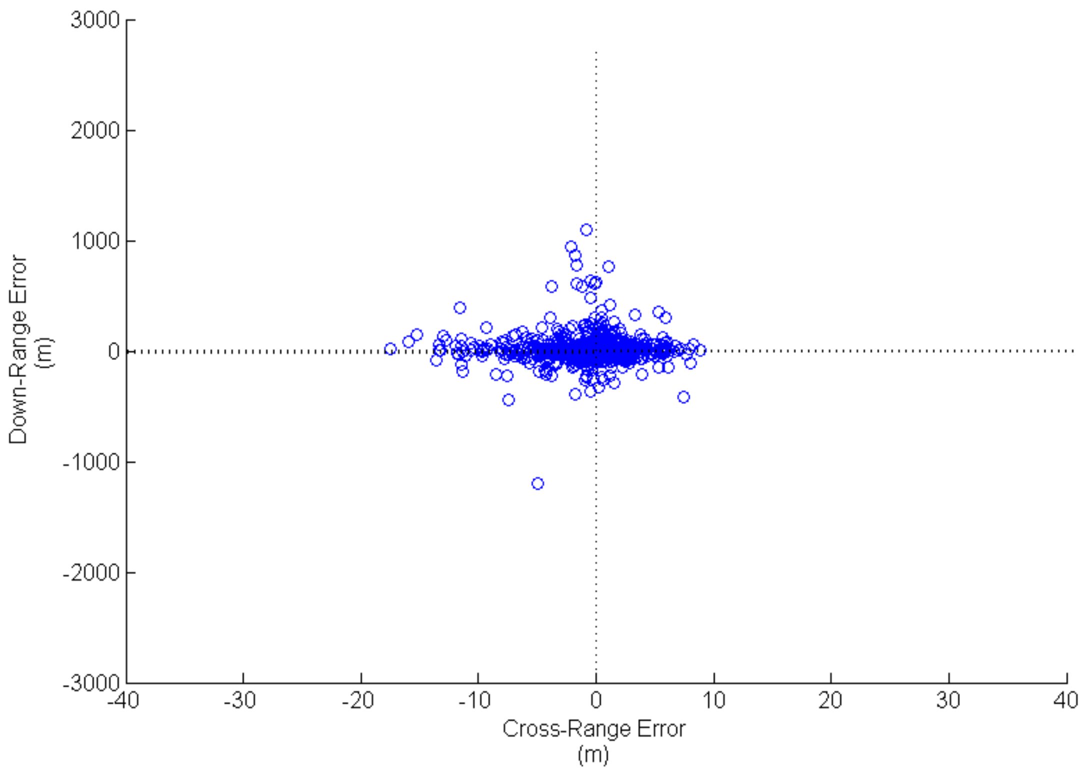

Figure 34: The Active Launcher Impact Dispersion

4.2.2 The Fixed Launcher

For the fixed launcher, there was no statistically significant correlation between errors and the variables except for reference pitch angle, horizontal distance, and altitude. That indicates that increases or decreases in these variables do not significantly relate to increases or decreases in errors. Furthermore, only a weak correlation was shown between errors and the horizontal distance, at 0.256. In fact, these small correlation values are negligible. It is likely that, again, these results mean that errors occurred due to pilot commands. The SPSS output for correlations is given in Table 16.

Table 16: Error Correlations of the Fixed Launcher

Correlations								
		Hel. Pitch Angle	**Reference Pitch Angle**	**Horz. Dist.**	**Vert. Dist.**	**Alt.**	**IAS**	**# of Fired**
Error	**Pearson Correlation**	−0.057	0.204**	0.256**	0.070	0.123**	−0.036	−0.005
	Sig. (2-tailed)	0.220	0.000	0.000	0.130	0.007	.432	0.912
	N	471	471	471	471	471	471	471
** Correlation is significant at the 0.01 level (2-tailed).								
* Correlation is significant at the 0.05 level (2-tailed).								

The impact positions of the rockets were standardized and scaled to zero–zero coordinates to demonstrate the dispersion for each firing. In this instance, 471 rockets were fired at distances varying from 986 meters to 8,570 meters. The impact distributions are shown in Figure 35, and pilot errors can be clearly seen. The miss distance was expected to be in a range between 50 meters and 100 meters for both down-range and cross-range. However, the difficult handling of the simulator and the motionless flight degraded the pilot’s situational awareness. Further, the cyclic was too sensitive, and it was difficult to control the helicopter in the pitch axis. In addition, the helicopter decelerated too quickly, causing the pilot to lose control at times during the simulation. It is safe to assume that for real firing sessions, the dispersion will be better than the results obtained in this study.

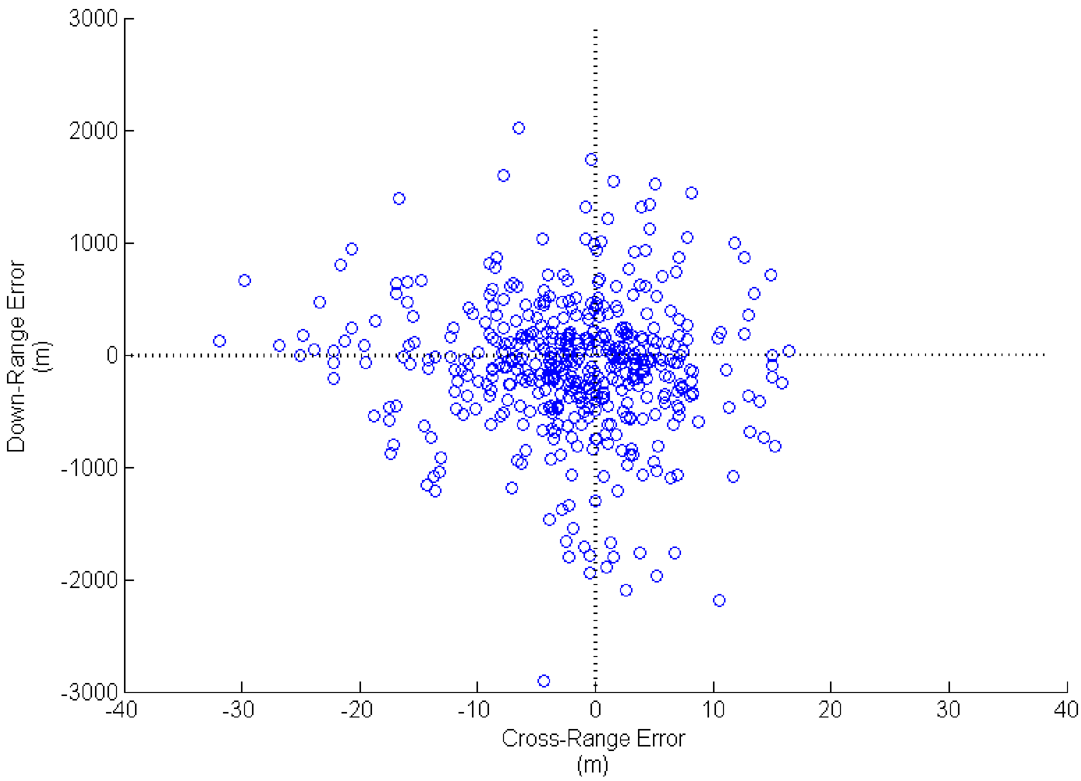

Figure 35: The Fixed Launcher Impact Dispersion

4.3 Accuracy of the Fixed Launcher

4.3.1 Circular Error of Probability

In ballistics, CEP is a measure of a weapon system's accuracy. The radius of the impact distribution, which is centered on the mean, includes the impact points of 50% of the rounds [29]. A simple formula for calculation of CEP that can be found in the literature is shown in Equation 38, below, where σ is the standard deviation of the cross-range and down-range errors.

$$CEP = 0.5887(\sigma_X + \sigma_Y) \qquad (38)$$

To calculate CEP, the data must be normally distributed [30]. Thus, outliers were removed from the data. For data with more than 29 values, the Kolmogorov–

Smirnov sig. value must be greater than 0.05 [24]. According to Table 17 below, the fixed launcher impact distribution was normally distributed.

Table 17 : Test of Normality

	Kolmogorov–Smirnov[a]		
	Statistic	df	Sig.
Down-Range Error	0.041	395	0.105
Cross-Range Error	0.071	395	0.155

a. Lilliefors significance correction.

** This is the lower bound of true significance.

The standard deviation of down-range error was $\sigma_y = 372.36$, and for the cross-range error, it was $\sigma_x = 19.50$. From Equation 38, the active launcher's CEP was found to be 230.68 meters.

CEP was calculated for distances to the target between 1,800 meters and 4,500 meters and heights above the target ranging from 0 feet to 800 feet. Because there was insufficient data to calculate the CEP, the ranges were changed as mentioned herein. Outliers and the data with very high errors caused by the pilot were also removed. The resulting calculated CEP was accepted as the true value for this study. Results of a test of normality for the data are given in Table 18.

Table 18: Test of Normality

	Kolmogorov–Smirnov[a]		
	Statistic	df	Sig.
Down-Range Error	0.089	39	0.200*
Cross-Range Error	0.115	39	0.200*

a. Lilliefors significance correction.

* This is the lower bound of true significance.

The standard deviation of down-range error was $\sigma_y = 150$, and for cross-range error, it was $\sigma_x = 30.39$. Using Equation 38, the active launcher's CEP was found to be 106.19 meters.

However, in a study by Hawley [31], the CEP of Hydra-70 rockets (38 rounds fired) was calculated to be 29 mils at a 2,000-meter range distance. According to Hawley, the CEP of a fixed launcher is 58 meters, which is half of the results in this study.

4.3.2 The Probability of a Hit

The M151 HE is an antipersonnel, anti-material warhead that has a 10-meter bursting radius. However, high-velocity fragments can produce a lethality radius in excess of 50 meters.

The probability of a hit can be calculated by using the formula in Equation 39 [29].

$$P = 1 - \exp(-0.6931 * [R^2 / CEP^2]) \quad , \tag{39}$$

where

- P = the probability of a hit,
- R = the radius of the target, and
- CEP = the circular error of probability of the weapon.

If the radius of the target is 50 meters, the probability of a hit can be determined from Equation 39 to be P_1=3.18%.

4.4 Accuracy of the Active Launcher

4.4.1 Circular Error of Probability

As can be seen in Table 19, the remaining 483 values were all normally distributed.

Table 19: Test of Normality

	Kolmogorov–Smirnov[a]		
	Statistic	df	Sig.
Down-Range Error	0.025	483	0.200*
Cross-Range Error	0.023	483	0.200*

a. Lilliefors significance correction.

* This is the lower bound of true significance.

The standard deviation of the down-range error was $\sigma_y = 43.85$, and for the cross-range error, it was $\sigma_x = 10.28$. From Equation 38, the active launcher's CEP was found to be 31.86 meters.

4.4.1.1 CEP for 2,000–3,000 Meters

As compared to the study by Hawley [31], the CEP of the proposed system's horizontal distance to the target was limited to 2,000–3,000 meters, and the height above the target was limited to 0 to 500 feet. The new data set had 30 records when the outliers were removed. Test of normality results are given below in Table 20.

Table 20: Test of Normality

	Kolmogorov–Smirnov[a]		
	Statistic	df	Sig.
Down-Range Error	0.119	30	0.200*
Cross-Range Error	0.117	30	0.200*

a. Lilliefors significance correction.

* This is the lower bound of true significance.

The standard deviation of the down-range error was $\sigma_y = 59.66$, and for the cross-range error, it was $\sigma_x = 13.58$. From Equation 38, the active launcher's CEP was found to be 43.11 meters.

4.4.1.2 CEP for 3,000–4,000 meters

The same process was applied for the following ranges. Test of normality results are given below in Table 21.

Table 21: Test of Normality

	Kolmogorov–Smirnov[a]		
	Statistic	df	Sig.
Cross-Range Error	0.112	29	0.200*
Down-Range Error	0.126	29	0.200*

a. Lilliefors significance correction.

* This is the lower bound of true significance.

he standard deviation of the down-range error was $\sigma_y = 45.35$, and for the cross-range error, it was $\sigma_x = 17.28$. From Equation 38, the active launcher's CEP was found to be 36.87 meters.

4.4.1.3 CEP for 4,000–5,000 meters

Test of normality results for the given range data are given below in Table 22. The standard deviation of the down-range error was $\sigma_y = 42.06$, and for the cross-range error, it was $\sigma_x = 14.45$. From Equation 38, the active launcher's CEP was found to be 33.27 meters.

Table 22: Test of Normality

	Kolmogorov–Smirnov[a]		
	Statistic	df	Sig.
Down-Range Error	0.126	29	0.200*
Cross-Range Error	0.112	29	0.200*

a. Lilliefors significance correction.

* This is the lower bound of true significance.

4.4.2 The Probability of a Hit

If the radius of the target is 50 meters, the probability of a hit can be determined using Equation 39 for the given ranges as shown in Table 23:

Table 23: Probability of a Hit

Ranges	Probability of a Hit
0–9,000	81.72%
2,000–3,000	60.66%
3,000–4,000	71.88%
4,000–5,000	78.97%

Recall the result of the fixed launcher in this study was found to be P_1=3.18%. On the other hand, according to Hawley's CEP result, the probability of a hit becomes P=40.11%.

4.5 Comparison

As expected, when using the active rocket launcher, down-range performance was greatly improved. Conversely, the down-range error in this study was high with the fixed launcher due to lack of a controller that applied in the yaw direction and pilot command errors. Especially, while reference pitch angle was above 5 degrees, error was relatively high. On the other hand, cross-range errors were nearly the same with both the active and the fixed launchers. The average absolute error of the fixed launcher was 445.51 meters whereas the active launcher was only 59.82 meters. It can be said that the active launcher enhanced the down-range dispersion ratio by 86.57%.

Furthermore, CEP and probability of a hit also greatly improved with the active launcher. A comparison of the results found in previous sections is presented below on Table 24.

Table 24: Comparison of the Results

	Circular Error of Probability	**Probability of a Hit**
Active Launcher	31.86 meters	81.72%
Fixed Launcher	106.19 meters	14.19%
Results of Hawley	58 meters	40.11%

CHAPTER 5

CONCLUSION AND FUTURE WORK

The main motivation behind this study was to design an active rocket launcher system that can cancel out disturbances to rocket launchers that occurs during flight due to turbulence and pilot errors. The necessity of using pitch delivery charts creates more preflight preparation and an extra burden on the pilot during operations. What's more, during a target engagement, a little cyclic error or a little turbulence may cause a miss. To overcome these problems, new systems are being adapted to rockets, such as adding a laser guidance kit, that make these new weapons far more expensive than unguided rocket systems. A promising alternative is an active rocket launcher system that is able to automate the pitch angle to satisfy the elevation for high hit probabilities and high kill ratios without changing the helicopter's pitch attitude.

In order to develop an effective weapons system for this study, a rocket trajectory simulator based mainly on thrust and drag was built in MATLAB. To minimize errors and to include scenarios and flight conditions that pilots encounter during operations, parameter intervals were specified in great detail as much as possible. By analyzing the relationship between pitch angle and the other variables and how they affect the required elevation, a polynomial was estimated and solved in SPSS 17 to compile a custom regression model. The regression model was run with the complete data, and the results were compared with the rocket trajectory model.

Because the aim was to have the system tested on a flight simulator by a well-trained and experienced attack helicopter pilot, it was necessary to build a simulation of the launcher's physical model on CATIA for several launcher loads. The dynamics of the launcher loads were calculated separately and, when the rockets were fired in order, together. For every load condition of the launcher in firing order, different gains are calculated, which could be implemented in a manufactured system with a gain scheduler. For the active launcher approach, it was assumed that a servo motor was mounted on the geometric center of the launcher to execute the elevation control process for rocket engagement.

In order to implement an effectively controlled rocket launcher platform, a PID controller was developed. Implementing a robust PID control is simpler and requires less computational effort in comparison to modern controllers. Since the active rocket launcher system has not thus far been used in any attack helicopter system, a PID controller was more suitable for adapting to the industrial product being studied.

Finally, two experiments were conducted in the simulator by the first author, who is currently an attack helicopter pilot, at different velocities, altitudes, air densities, and target parameters. The performance of the system was observed by giving the required pitch angle as a reference to the rocket launcher, gathering data on tracking ability, and comparing the results with the fixed launcher firings. The impact points of both simulation runs were calculated and remapped to calculate the circular error of probability and the probability of a hit. These accuracy factors were compared to each other as well as being compared to results from the literature of a study that used the same rocket model. The results clearly show that the launcher is able to track the reference pitch angle signal obtained by the built regression model during the simulation. This resulted in the impact dispersion of the active rocket launcher being greatly improved; obtaining a high CEP ratio that was appreciably close to that of a guided system in an unguided one. The active launcher system could be an ideal cost-effective solution for attack helicopter pilots who prefer to use “fire and forget” missiles in combat situations for the sake of their own safety.

More advanced models that use different controllers will be studied in the future and implemented in the current research. The proposed system will be compared with a modern automatic flight-controlled attack helicopter simulation that can adjust the helicopter to the target in order to tilt the launcher. The ballistic solution algorithm will also be improved with the addition of parameters such as, for example, wind, rotor downwash, and humidity. The robustness and applicability of the system will be tested in a different attack helicopter simulator with different pilots. Finally, modern control methods, such as LQR, adaptive flight control, and predictive algorithms will be implemented with the system, and their performance results will be compared with the system studied in this thesis.

REFERENCES

[1]R. D. Joyce. *Unguided rocket employment: why we must update marine corps rotary wing attack training.* United States Marine Corps, Quantico, 2008.

[2] M. Khalil, H. Abdalla, and O. Kamal. Trajectory prediction for a typical fin stabilized artillery rocket. *Int. Conf. Aerosp. Sci. Aviat. Technol*., pp. 1–14, 2009.

[3] *Tactical employment AH-1W(U) NTTP 3-22.3-AH1W*. Department of the Navy, Washington, 2003.

[4] *Flight manual navy model AH-1W helicopter*. Department of the Navy, Washington, 2007.

[5] M. S. P. Haney. *De-fanging the cobra: staking the future on unproven weapons.* globalsecurity.org,1995. `http://www.globalsecurity.org/military/library/report/1995/HSP.htm.` last visited on August 2017

[6] H. A. Morse. Some practical aspects of rotor wake effects on rocket accuracy. In *The Helicopter Downwash on Free Projectiles Conference,1978.* pp. 32–53, 1978.

[7] B. Z. Jenkins. The perturbed flow environment about helicopters and its effect on free rockets. pp. 6–32, 1978.

[8] S. Osder, M. Douglas, and H. Company. Integrated flight / fire control for attack helicopters, *IEEE AES Systems Magazine* pp. 17–23, 1992.

[9] J. H. Blakelock. Design and analysis of a digitally controlled integrated flight/firecontrol system. *Journal of Guidance, Control, and Dynamics*, Vol. 6, No. 4, pp. 251-257,1983.

[10] Z. Koruba. Control and correction of a gyroscopic platform mounted in a flying object. *Journal of Theoretical and Applied Mechanics*, vol. 45, no. 1, pp. 41–51, 2007.

[11] Z. Koruba, Z. Dziopa, and I. Krzysztofik. Dynamics of a controlled anti-aircraft missile launcher mounted on a moveable base. *Journal of Theoretical and Applied Mechanics*, vol. 48, no. 2, pp. 279–295, 2010.

[12] Z. Koruba, D. Koruba, and I. Krzysztofik. Dynamics and controls of a gyroscope-stabilized platform in a self-propelled anti-aircraft system. *Journal of Theoretical and Applied Mechanics*, vol. 48, no. 1, pp. 5–26, 2010.

[13] N. D. Parkpoom Ch. System identification and control the azimuth angle of the platform of MLRS by PID controller. *International Journal of Computer, Electrical, Automation, Control and Information Engineering*, vol. 6, no. 9, pp. 1120–1123, 2012.

[14] Ö. Gümüşay. *Intelligent stabilization control of turret subsystems under disturbances from unstructured terrain.* Middle East Technical University, Ankara, 2006.

[15] Ö. Kapulu. *Separation simulation for helicopter external stores and generation of safe separation envelopes.* Middle East Technical University, Ankara, 2015.

[16] *AH-1W Naval Aviation Technical Information Product NTRP 3-22.4 AH-1W*, Department of the Navy, Washington, 2008.

[17] W. Charubhun, P. Chusilp, and N. Nutkumhang. Effects of aerodynamic coefficient uncertainties on trajectory simulation of a short-range solid propellant free rocket. *26th International Symposium On Ballistics.* Miami, 2011.

[18] K. K. Parsons. MATLAB Rocket Trajectory Simulation. `http://kevinkparsons.com/projects/matlab-rocket-trajectory-simulation.html`, last visited on, January 2017

[19] C. W. Dahike and G. Batiuk. *Hydra 70 MK 66 Aerodynamics and Roll Analysis*, TR-RDSS-90. US Army Missile Command, Redstone Arsenal, 1990.

[20] A. Massey and S. J. Miller. *Tests of Hypotheses Using Statistics*, Brown University, Providence, 2006.

[21] D. George and P. Mallary. *SPSS for windows step by step: a simple guide and reference, 17.0 update (10a ed.).* Pearson, Boston, 2010.

[22] B. S. Everitt and A. S. Skondal. *The cambridge dictionary of statistics.* Cambridge University Press, Cambridge, 2006.

[23] H. Pham. *Springer Handbook of Engineering Statistics*. Springer, Berlin, 2006.

[24] S. Landau and B. Everitt. *A handbook of statistical analyses using SPSS.*, Chapman & Hall/CRC, Washington, 2004.

[25] S. a van de Geer. Least Squares Estimation. Encyclopedia of Statistics in Behavioral Science, vol. 2, pp. 1041–1045, 2005. John Wiley & Sons, Ltd, Chichester, 2005

[26] J. Obermark and K. Key. *Verification of simulation results using scale model flight test trajectories*, TR-AMR-AE-04-01. Redstone Arsenal, 2004.

[27] E. Akgül. *PID and LQR control of a planar head stabilization platform.* Middle East Technical University, Ankara, 2011.

[28] D. Yılmaz and I. Yavrucuk. Development of a flight dynamics model for a UH-1H helicopter simulator. In *4th Ankara International Aerospace. Conference*. vol. AIAC-2007-, pp. 1–14, 2007.

[29] A. Nia. *ADS-44-HDBK Aeronautical Design Standard Handbook Armament Airworthiness Qualification For U.S. Army Aircraft.* April 1990 CAGE Code 81996. Army Aviation and Missile Research, Development and Engineering Center, Redstone Arsenal, 2006.

[30] G. M. Siouris, *Missile guidance and control systems,* Springer, New York, 2004.

[31] E. Hawley. *Advanced propulsion concepts for the hydra-70 rocket system.* Indian Head Division, Naval Surface Warfare Center, Washington, 2003.